2005-12

Transport imaging for the study of quantum scattering phenomena in next generation semiconductor devices

Bradley, Frank Mitchell

Monterey, California. Naval Postgraduate School

https://hdl.handle.net/10945/1851

NAVAL POSTGRADUATE SCHOOL

MONTEREY, CALIFORNIA

THESIS

TRANSPORT IMAGING FOR THE STUDY OF QUANTUM SCATTERING PHENOMENA IN NEXT GENERATION SEMICONDUCTOR DEVICES

by

Frank Mitchell Bradley

December 2005

Thesis Advisor:	Nancy M. Haegel
Second Reader:	James Luscombe

Approved for public release; distribution is unlimited

THIS PAGE INTENTIONALLY LEFT BLANK

REPORT DOCUMENTATION PAGE			*Form Approved OMB No. 0704-0188*
Public reporting burden for this collection of information is estimated to average 1 hour per response, including the time for reviewing instruction, searching existing data sources, gathering and maintaining the data needed, and completing and reviewing the collection of information. Send comments regarding this burden estimate or any other aspect of this collection of information, including suggestions for reducing this burden, to Washington headquarters Services, Directorate for Information Operations and Reports, 1215 Jefferson Davis Highway, Suite 1204, Arlington, VA 22202-4302, and to the Office of Management and Budget, Paperwork Reduction Project (0704-0188) Washington DC 20503.			
1. AGENCY USE ONLY *(Leave blank)*	**2. REPORT DATE** December, 2005	**3. REPORT TYPE AND DATES COVERED** Master's Thesis	
4. TITLE AND SUBTITLE: Transport Imaging for the Study of Quantum Scattering Phenomena in Next Generation Semiconductor Devices			**5. FUNDING NUMBERS**
6. AUTHOR(S) Frank Mitchell Bradley			
7. PERFORMING ORGANIZATION NAME(S) AND ADDRESS(ES) Naval Postgraduate School Monterey, CA 93943-5000			**8. PERFORMING ORGANIZATION REPORT NUMBER**
9. SPONSORING /MONITORING AGENCY NAME(S) AND ADDRESS(ES) National Science Foundation Research Corporation CC4411			**10. SPONSORING/MONITORING AGENCY REPORT NUMBER** DMR 20033397
11. SUPPLEMENTARY NOTES The views expressed in this thesis are those of the author and do not reflect the official policy or position of the Department of Defense or the U.S. Government.			
12a. DISTRIBUTION / AVAILABILITY STATEMENT Approved for public release; distribution is unlimited			**12b. DISTRIBUTION CODE**

13. ABSTRACT (maximum 200 words)

The minority carrier diffusion length is a critical parameter in the development of next generation Heterostructure Bipolar Transistors (HBT) and highly efficient solar cells. A novel technique has been developed utilizing direct imaging of electron/hole recombination via an optical microscope and a high sensitivity charge coupled device coupled to a scanning electron microscope to capture spatial information about the transport behavior (diffusion lengths/drift lengths) in luminescent solid state materials. In this work, a numerical model was developed to do a multi-parameter least squares analysis of transport images. Results were applied to the study of transport in materials at the forefront of device technology that are affected by quantum scattering effects, where few reliable experimental measurements exist. The technique allows for easy localization of the measurement site, broad application to a range of materials and potential industrial automation to aid the development of high speed electronics for terahertz devices.

14. SUBJECT TERMS Minority carrier diffusion length, heterostructure bipolar transistors, transport imaging, heavily doped GaAs transport properties			**15. NUMBER OF PAGES** 113
			16. PRICE CODE
17. SECURITY CLASSIFICATION OF REPORT Unclassified	**18. SECURITY CLASSIFICATION OF THIS PAGE** Unclassified	**19. SECURITY CLASSIFICATION OF ABSTRACT** Unclassified	**20. LIMITATION OF ABSTRACT** UL

NSN 7540-01-280-5500 Standard Form 298 (Rev. 2-89)
Prescribed by ANSI Std. 239-18

THIS PAGE INTENTIONALLY LEFT BLANK

Approved for public release; distribution is unlimited

TRANSPORT IMAGING FOR THE STUDY OF QUANTUM SCATTERING PHENOMENA IN NEXT GENERATION SEMICONDUCTOR DEVICES

Frank M. Bradley
Lieutenant Commander, United States Navy
B.S., United States Naval Academy, 1991

Submitted in partial fulfillment of the
requirements for the degree of

MASTER OF SCIENCE IN PHYSICS

from the

NAVAL POSTGRADUATE SCHOOL
December 2005

Author: Frank Mitchell Bradley

Approved by: Nancy M. Haegel
Thesis Advisor

James Luscombe
Second Reader

James Luscombe
Chairman, Department of Physics

THIS PAGE INTENTIONALLY LEFT BLANK

ABSTRACT

The minority carrier diffusion length is a critical parameter in the development of next generation Heterostructure Bipolar Transistors (HBT) and highly efficient solar cells. A novel technique has been developed utilizing direct imaging of electron/hole recombination via an optical microscope and a high sensitivity charge coupled device coupled to a scanning electron microscope to capture spatial information about the transport behavior (diffusion lengths/drift lengths) in luminescent solid state materials. In this work, a numerical model was developed to do a multi-parameter least squares analysis of transport images. Results were applied to the study of transport in materials at the forefront of device technology that are affected by quantum scattering effects, where few reliable experimental measurements exist. The technique allows for easy localization of the measurement site, broad application to a range of materials and potential industrial automation to aid the development of high speed electronics for terahertz devices.

THIS PAGE INTENTIONALLY LEFT BLANK

TABLE OF CONTENTS

LIST OF FIGURES

LIST OF TABLES

THIS PAGE INTENTIONALLY LEFT BLANK

ACKNOWLEDGMENTS

Though times are good or be they unknowable
The names to be trusted are always the same.
A family as steady as the Redwoods of ages.
A God more present than the mind can conceive.
Friends and mentors in a variety of manners,
Have touched me in ways too deep to perceive.

A word to all who read this in wonder,
“Why would a man care so for science?”

For I have seen good and bad in abundance.
The good, more often, was forgotten by most,
But the evil withstands and calls us each one.
It either is answered or followed asunder.
And ignorance is surely the path of the latter.

I acknowledge those who will not stand idle.
I acknowledge those who are pressed to act.
I acknowledge those who in their dying,
Have given me life of spirit and mind.
I acknowledge those who have gone before me
Great warriors, scholars, kith and kin.

THIS PAGE INTENTIONALLY LEFT BLANK

I. INTRODUCTION

A. HISTORY

With the emergence of the transistor in 1947 came a revolution in military affairs (RMA) that has been evolving over the subsequent 59 years. Today, the battlefield and our daily lives are littered with electronic devices that do everything from helping us to see in the dark to enabling global communication links. The transistors that act at the foundation of these capabilities are able to perform faster and faster every “Moore cycle”. As the demand for faster processing in smaller electronics packages has grown, electronics makers have turned to a class of transistor called the Heterojunction Bipolar Transistor (HBT).

HBTs are transistors in which at least one of the two transistor interfaces is formed of two distinct materials [1]. The primary advantage of HBTs is their greater emitter efficiency, defined as the ratio of current injected into the emitter from an external source to the leakage current from the base to the emitter under active operation. This advantage results directly from the valence band discontinuity at the emitter-base heterojunction. The larger barrier to minority carrier injection from base to emitter allows for a substantial increase in the permissible doping level of the base layer of the HBT, which reduces sheet resistance and allows for thinner base layers without concern of emitter-collector leakage in the cutoff mode of operation. These advantages result in a faster base transit time, defined as the time required for the emitter injected carriers (minority carriers in the base) to diffuse across the base layer to the collector, and a faster switching speed for the HBT. A schematic and energy band diagram is shown in Figure 1 highlighting the valence and conduction band discontinuities.

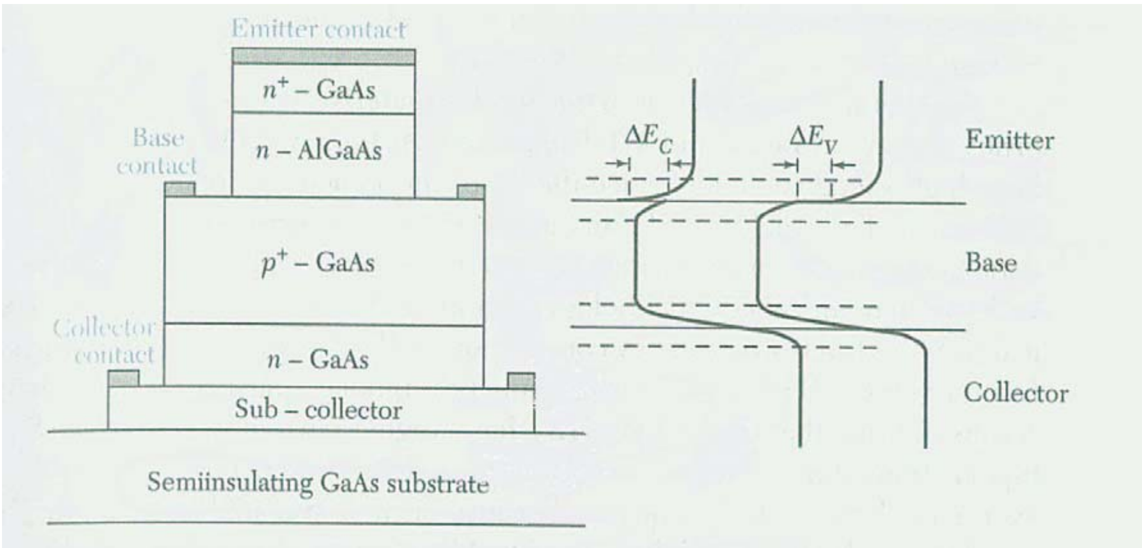

(a) (b)

Figure 1. (a) Schematic cross section of an HBT structure. (b) Energy band diagram of a HBT operated under active mode. (From Ref.[1])

The use of different materials to provide these junctions, while adding complexity to the design, adds significant power amplification benefits and switching speed advantages [3]. Figure 2 shows a history of progression of highest cutoff frequency (F_T) for various transistors over time. The cutoff frequency is defined as the frequency where current gain of one is achieved. It is noted that the maximum working frequency of these devices, $F_{\max}$, is the frequency where power gain becomes unity and is below F_T [4].

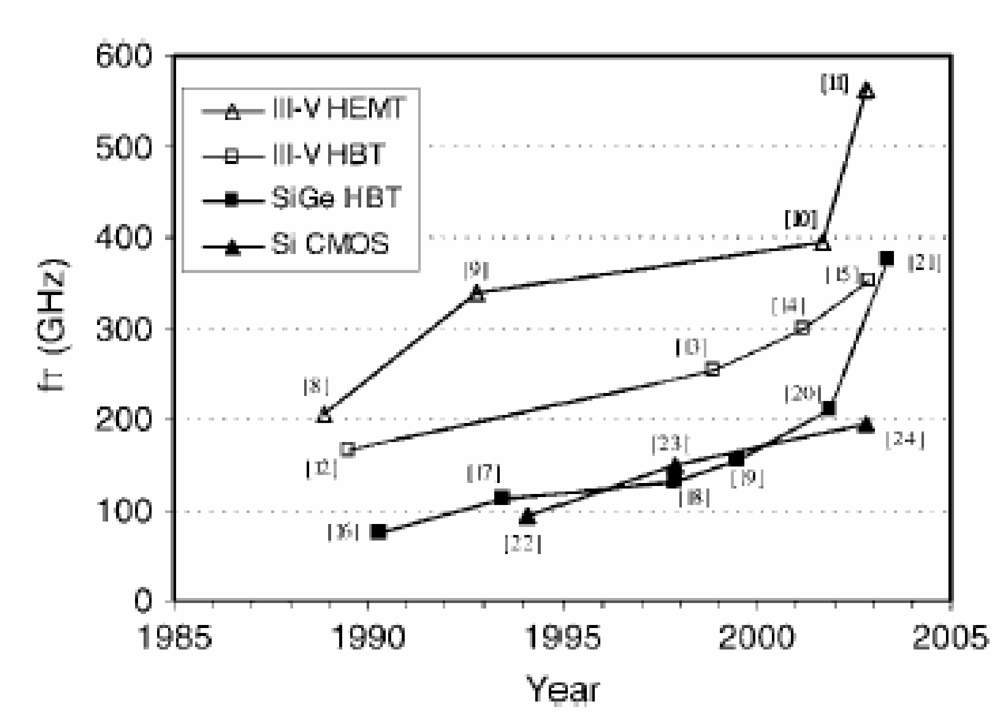

Figure 2. Trend of best achieved F_T for various transistors. (From Ref[4])

In order to achieve these frequencies of operation, manufacturers increasingly rely upon thinner, more heavily doped materials to propagate charge quickly and efficiently across the base to activate the transistor [1],[2],[5]. These increases in doping level and the shrinking of relative dimensions, in particular of the base layer, have coupled to bring about new and interesting regimes that operate on the edge of known macroscopically determined semiconductor transport properties. In order to effectively design and build the most efficient devices in these new highly doped low dimensional regimes, new techniques that can extract and model material properties on the sub-micrometer scale will be necessary [9].

B. MILITARY RELEVANCE

High speed electronics are important for a variety of military applications. The Terahertz frequency band, defined as the frequency range between 300 GHZ and three terahertz, is being explored for applications in medical diagnostic imaging, security imaging, and high bandwidth communications, just to name a few. A quote from a recent Defense Advanced Research Projects Agency (DARPA) Broad Agency Announcement (BAA) highlights what might be considered the most critical of these applications for our information centric battlespace.

> The continuing need by DoD for ultra-high bandwidth communications and sensing will require electronics that operate at THz frequencies. Given that advanced microwave satellite communication systems already operate near 60 GHz, the instantaneous bandwidth required to fully monitor the battlespace will certainly exceed 300 GHz early in the next century. All communication bottlenecks must be removed so that surveillance systems can relay their wideband measurements to other locations for real-time analysis [10].

Conventional electronic sources and receivers are limited by resistances, capacitances, and transit times, resulting in a significant attenuation of high frequency power. High power amplifiers based on HBTs are beginning to approach the realm of terahertz oscillations and may provide a simple semiconductor based solution for an integrated coherent terahertz source and detector. A greater understanding of the physics of electrical carrier transport in these highly doped, low dimensional structures will aid the development of these devices and provide manufacturers with more accurate models and predictive design tools.

C. THESIS OVERVIEW

In this thesis, (sponsored by National Science Foundation DMR 0203397) an application of a new technique for imaging charge transport is discussed [6-8]. A study of a series of low dimensional, heavily doped AlGaAs/GaAs heterostructures was conducted with an emphasis on the determination of the diffusion length of the minority carriers as a function of impurity doping. These results showed values of the minority carrier mobility that can only be explained with the incorporation of quantum mechanical scattering behavior at very high carrier concentrations. This appears to be the first direct measurement of diffusion lengths and minority carrier mobilities in this important material system [9]. Chapter II develops the mathematical model underpinning the transport of minority carriers in the low dimensional structures of interest. Chapter III briefly describes the experimental apparatus and the technique used to extract the material properties, while Chapter IV explores the theoretical limits of the model and demonstrates experimental evidence of those limits. In Chapter V the experimental evidence showing an increase in minority carrier mobility in heavily doped GaAs $\approx 10^{20}(cm^{-3})$ is presented, and the results are discussed in the context of existing theoretical work.

THIS PAGE INTENTIONALLY LEFT BLANK

II. TRANSPORT IMAGING IN THE TWO DIMENSIONAL LIMIT

A. OVERVIEW

SEM charge transport imaging combines two microscopes – a scanning electron microscope (SEM) to provide high resolution charge generation and an optical microscope to image the transport of charge. It can be performed in any material with a luminescent signature associated with charge recombination. In its basic operation, non-equilibrium minority carriers are injected into the luminescent semiconductor material by the SEM and the resulting radiative recombination is imaged through the optical microscope (OM). Analysis of the captured image allows quantitative, localized transport measurements.

One application for this technique is as a means to perform contact-free measurements of minority carrier diffusion lengths. This is a key parameter for many devices, including solar cells, photoconductors, and HBTs, as discussed in Chapter I. More conventional techniques for measuring diffusion lengths are generally limited by the need for contacts and the spatial averaging that occurs in macroscopic electrical measurements. Transport imaging can determine this important materials parameter directly from a single, zero bias luminescent spot image, particularly for samples in the 2D (thin layer) limit.

B. MODELING LIMITATIONS AND ASSUMPTIONS

In specific application to the materials of interest from Chapter I we consider the case where a thin sample is doped and the charge generation rate is sufficiently low so that we are able to model the transport of minority carriers in an approximately constant distribution of majority carriers. For example, in doped samples of a 1 μm active layer AlGaAs/GaAs heterostructure, with incident electrons of ~ 15 keV, this means an electron beam current of ~1×10^{-8} A or less for material doped at ~1×10^{18} cm^{-3}. This approximation is made by assuming a highest value generation rate G of G ~ E_{acc}/E_i, where E_{acc} is the incident electron energy and E_i is the energy required to produce an electron/hole pair. For energies in the ~ 5 – 40 keV range, one can approximate $E_i \sim 3E_g$ for a bandgap of E_g [12]. The total carrier population $\Delta n \sim \Delta p$ created then per electron is $G\tau$. We approximate here a lifetime of τ~1 ns and a probe current of 1 nA, but the results can be scaled accordingly. In this example our ratio of resident majority carriers to minority carriers is on the order of 100. Therefore, our low injection limit is valid. The generation volume radius for the electrons was approximated from the model of Kanaya–Okayama as ~ 1.5 μm in GaAs at 30 keV, with a hemispherical generation volume [13]. For more heavily doped materials, or shorter lifetime materials, one could use higher probe currents. Transport imaging can be performed outside these limits with more sophisticated modeling, but we will restrict ourselves to the low injection case for the analysis that follows.

C. MATHEMATICAL MODEL DEVELOPMENT

For cases where the diffusion length is comparable to or greater than our system resolution, diffusion of the minority carriers will broaden the luminescent spot. The extent of optical emission then becomes a function of minority carrier diffusion length and the diffusion length can be directly extracted from the optical emission image. This approach cannot be easily applied to bulk/thick samples due to the generation volume created by incident electrons and the relatively weak dependence of the minority carrier distribution on diffusion length in 3D. However, since many new materials and devices utilize primarily thin films, (eg, heterostructures, quantum wells and specifically the base regions of HBTs) the range of applications for contact-free diffusion length measurements is large.

In order to extract the diffusion length from the optical image, we model a steady state distribution of minority carriers created by a generation region of finite extent. The SEM beam, operated in a low injection configuration, is the source of the generation region, and our 2D assumption is based upon the relatively thin depth of the active region compared with its extent in the other two dimensions.

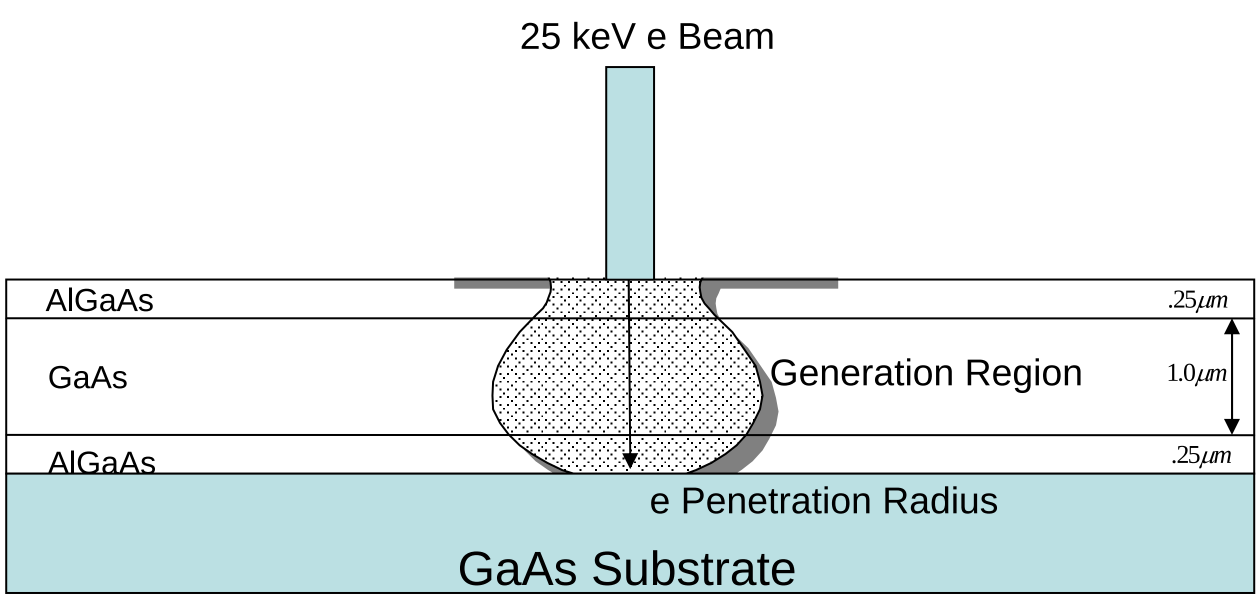

Figure 3. E-Beam/Sample interaction schematic

The sample reaches steady state very quickly, and we will describe the distribution of the minority carriers in the optically active GaAs layer. The heterostructure has been modulation doped with Be (p-type), and the minority carriers are electrons.

Beginning with the continuity equation for electrons in a p-type material:

$$(1) \qquad \frac{dn}{dt} = G_n - U_n + \frac{1}{q}\vec{\nabla}\cdot\vec{J}_n$$

where G_n is the generation rate [$1/cm^3 s$].

U_n is the recombination rate = $\frac{\Delta n}{\tau_n}$ for low injection.

$\frac{dn}{dt}$ is the time rate of change of electrons per volume per second.

$\vec{J}_n$ is the current density vector

Δn is the number of excess minority carriers available for recombination

τ_n is the lifetime for electrons

Defining the steady state current density for carriers:

$$(2) \qquad \vec{J}_n = q\mu_n n\vec{E} + qD_n\vec{\nabla}n \quad [\frac{C}{cm^2 s}]$$

μ_n is the mobility of electrons in GaAs and

$\vec{E}$ is the externally applied electric field.

D_n is the diffusion coefficient for electrons further related to the Diffusion Length by:

(3) $$L = \sqrt{D_n \tau_n}$$

By combining the equations above we get:

(4) $$\frac{dn}{dt} = G_n - \frac{n}{\tau_n} + \vec{\nabla} \cdot \left[\mu_n n \vec{E} - \frac{L^2}{\tau_n} \vec{\nabla} n \right]$$

By our assumption we are at steady state and therefore the time rate of change of the electron distribution is zero. Now, assume a constant E field in the x direction so that $\vec{E} = q\mathrm{E}\vec{x}$, and Equation (4) becomes:

(4.5) $$0 = G_n - \frac{n}{\tau_n} + \mu_n E \frac{dn}{dx} + \frac{L^2}{\tau_n} \vec{\nabla}^2 n$$

By multiplying through by $\tau_n \big/ L^2$ and making the substitution: $S = \mu \tau E$, where S is the drift length, we get Equation (5).

(5) $$\vec{\nabla}^2 n + \frac{S}{L^2} n_x - \frac{1}{L^2} n = \frac{-G_n \tau_n}{L^2}$$

1. Generation Region

Here we make a digression to discuss the nature of $G_n \tau_n$, the steady state generation distribution created by the balance between the continuous SEM injection and recombination within the sample. After Donolato and Venturi we can define the distribution as a depth dosed Gaussian distribution [15].

(6) $$g(r,z;R) = \frac{g_o}{R} \frac{\Lambda\left(\frac{z}{R}\right)}{2\pi\sigma^2(z,R)} e^{\frac{-r^2}{2\sigma^2(z,R)}}$$

Here the key feature of the distribution is the variance σ being formed of two linearly independent factors:

(7) $$\sigma^2(z,R) = \sigma_o{}^2 + \sigma_s{}^2(z,R)$$

where σ_o is the variance of the beam and σ_s is the spread of the primary and secondary electrons in the sample due to scattering. z and R are the depth coordinate and the primary electron range respectively. R is a function of beam energy and the atomic number and density of the target material.

Let σ_o be the measure of the diameter of the circle within the beam that contains 50% of the total beam current, or d=beam diameter=1.67σ_o. From empirical measurements we can assume that the lateral scattering variance $\sigma_s \approx 0.1\frac{z^3}{R}$ [15]. R can be determined from ref [16] for a beam energy of 15keV in GaAs to be approximately $\approx 1.5\mu m$, and $\approx 2.0\mu m$ for a 25 keV beam energy. Though there is variation in the generation shape as shown in Figure 3 as a function of the depth (z) we approximate the variance as constant for the generation region in our active layer. Assuming an average depth of R/2 the generation variance becomes:

(8) $$\sigma\ (z,R) = \sqrt{.36d^2 + 0.1\left(\frac{R}{2}\right)^2}$$

For a 15 keV beam energy and d=$1.75\mu m$, $\sigma_{gen} = 1.06\mu m$, and the radius within which 99% of the charge will be generated is $2\sqrt{2}\sigma = 3\mu m$. This 99% value will define the limits of our source region for numerical integration in later sections.

We define our generation function for the source term and normalize the output to 1 using Equation (6):

$$(9) \qquad g(r') = e^{\frac{-r'^2}{2\sigma^2}}$$

2. Green's Function Solution

Returning to the differential Equation (5) with the inclusion of the source function, Equation (9):

$$(10) \quad \vec{\nabla}^2 n + \frac{S}{L^2} n_x - \frac{1}{L^2} n = \frac{-1}{L^2} e^{\frac{-r'^2}{2\sigma^2}}$$

By the use of an integration factor we can conduct a change of variables to eliminate the n_x term thereby making Equation (10) into the Helmholtz equation. Substituting:

(11) $n(x,y) = w(x,y)e^{ax}$ into (10) and combining terms we get:

$$(12) \qquad e^{ax}\left(w_{xx} + w_{yy} + 2aw_x + a^2 w\right) + \frac{S}{L^2} e^{ax}\left(w_x + aw\right) - \frac{1}{L^2} e^{ax} w = \frac{-1}{L^2} e^{\frac{-r'^2}{2\sigma^2}}$$

Combining like terms and dividing through by the exponential:

$$w_{xx} + w_{yy} + w_x\left(2a + \frac{S}{L^2}\right) + w\left(a^2 + \frac{Sa}{L^2} - \frac{1}{L^2}\right) = \frac{-1}{L^2} e^{\frac{-r'^2}{2\sigma^2}} e^{-ax}$$

Now we choose $2a + \frac{S}{L^2} = 0$ or $a = -\frac{S}{2L^2}$ in order to eliminate the derivative term to obtain:

$$(13) \qquad w_{xx} + w_{yy} - \frac{S^2 + 4L^2}{4L^4} w = \frac{-1}{L^2} e^{\frac{Sx}{2L^2}} e^{\frac{-r'^2}{2\sigma^2}}$$

which is nothing more than the Helmholtz equation where the Helmholtz operator is : $\nabla^2 + K^2$ and $K = i\frac{\sqrt{S^2+4L^2}}{2L^2}$.

Recognizing that the Green's Function for the Helmholtz operator is the zeroth order Bessell Function of the second kind [16],

$$G(r;r') = \frac{1}{2\pi} K_o\left(k\left|r-r'\right|\right) \tag{14}$$

where k is the real part of K: $k = \frac{\sqrt{S^2+4L^2}}{2L^2}$.

The general solution to a Green's Function problem is

$$w(x,y) = \int_0^\infty G(r;r')\frac{1}{L^2}e^{\frac{Sx'}{2L^2}}e^{\frac{-r'^2}{2\sigma^2}}dr'$$

Returning to the solution for the electron distribution (n) by the substitution: $n(x,y) = w(x,y)e^{ax}$ or $n(x,y) = w(x,y)e^{\frac{-S}{2L^2}x}$

Now,

$$n(x,y) = \frac{1}{2\pi}\frac{1}{L^2}\int_0^\infty K_o\left(\frac{\sqrt{S^2+4L^2}}{2L^2}\left|r-r'\right|\right)e^{\frac{Sx'}{2L^2}}e^{\frac{-Sx}{2L^2}}e^{\frac{-r'^2}{2\sigma^2}}dr' \tag{15}$$

By defining our limits of integration equal to the radius which contains 99% of the generation region's minority carriers as described by the Gaussian distribution in Equation (8) our model for the minority carrier distribution including diffusion and drift in 2D becomes:

$$n(x,y) = \frac{1}{2\pi L^2}\int_0^{2\sqrt{2}\sigma} K_o\left(\frac{\sqrt{S^2+4L^2}}{2L^2}\left|r-r'\right|\right)e^{\frac{S(x'-x)}{2L^2}}e^{\frac{-r'^2}{2\sigma^2}}dr' \tag{16}$$

The algorithm in Appendix A.5 is a Matlab coded version of this solution using a double quadrature numerical integration scheme to calculate the distribution of carriers as they drift/diffuse from the finite area defined by the Gaussian generation function (9) and bounded by the circle of radius $2\sqrt{2}\sigma$.

THIS PAGE INTENTIONALLY LEFT BLANK

III. EXPERIMENTAL APPARATUS

A. INTRODUCTION

The minority carrier distribution in a semiconductor sample reveals information regarding the transport properties of the material itself. As shown in the previous chapter the diffusion length of the minority carriers determines the shape of that distribution. The novelty of the Transport Imaging technique is the extraction of the salient aspects of that distribution from an actual sample in a controlled and flexible manner. By combining the charge injection and high resolution electron imaging capabilities of a Scanning Electron Microscope (SEM) with the optical resolution of a Silicon Charge Coupled Device (CCD) Camera, accurate spatial representations of these distributions are captured and analyzed. A custom software solution allows for the analysis of these images and the fitting of the experimental data to the mathematical model's predictions.

B. APPARATUS DESCRIPTION

The charge transport imaging instrument combines two independent microscopes – a JEOL SEM (See Table 1 for instrument specifications) for generating charge and an optical microscope (OM) for collecting and imaging the luminescence emitted from the recombination process. Using a retractable arm, the OM is placed directly under the pole piece in the SEM, allowing the electron beam to pass through the center of the first optical collecting surface. The initial demonstration system modifies an OM attachment for the JEOL SEM that was originally designed to allow the fine adjustment of sample height required for wavelength dispersive X-ray spectroscopy (WDS). WDS provides higher energy resolution than traditional energy dispersive X-ray analysis (EDX) and requires sensitive control of sample height in order to maintain proper conditions for multiple diffraction angles. OMs designed for this purpose have short focal lengths and are normally used in conjunction with a lamp source and low sensitivity near-IR/visible imager.

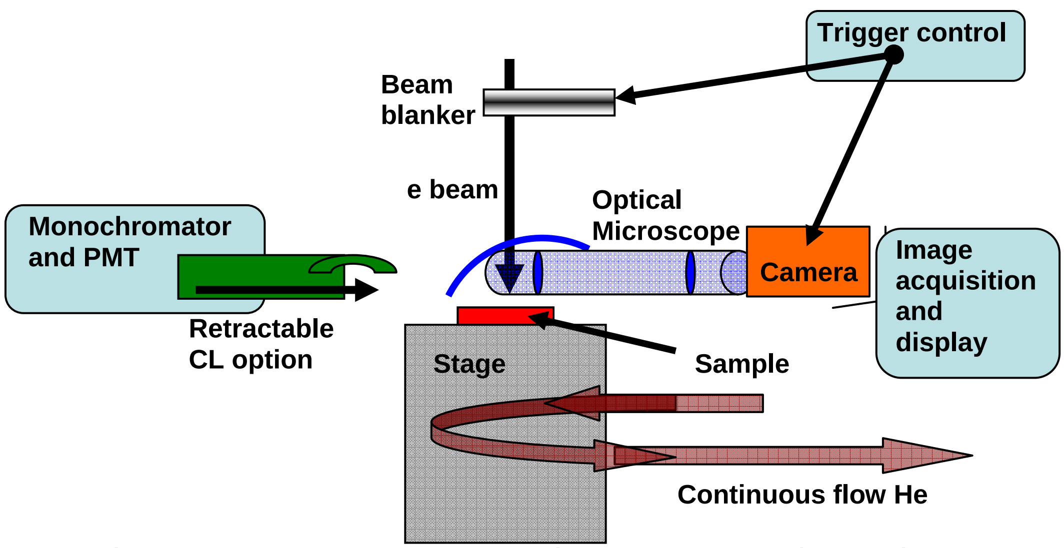

Figure 4. Transport Imaging System Schematic

A schematic of the system is shown in Figure 4. In addition to the charge transport imaging microscope, the instrument is equipped with standard CL capability using a Gatan (formerly Oxford Instruments) system with a parabolic mirror, ¼ m monochromator and TE cooled GaAs PMT as the detector. Beam blanking capability exists for future time resolved work. Finally, the instrument has a liquid helium cooled stage, so that transport imaging and conventional CL can be performed over a temperature range from 300 to ~ 5 K. The system uses continuous flow liquid He, with the sample stage inside the SEM mounted in a cold finger configuration.

Variable accelerating voltage; 200 to 40,000V
Variable probe current; 1x10E-8 to 1x10E-12 Amps
Maximum sample size of 6" in any one dimension
Working distances; 8 to 48mm
Sample rotation; 360º
Sample tilting 90º
Variable magnification; 10x to 300,000x
Maximum resolution; 10 nm
Secondary and Backscattered Electron detectors
Equipped with EDS capable of detecting Carbon and forming X-ray maps of composition; composition to within 0.1 wt%
Integrated digital imaging system
Noise reduction through frame averaging
Image capture and export in electronic form (TIFF
Low cost, medium quality thermal printouts
High quality, medium cost Polaroid type 55 film containing both negative and positive

Table 1. Table 1. JEOL 840A Specifications (From [11])

For transport imaging, the OM is used in a passive detection mode, detecting light emitted directly from the sample using a high sensitivity cooled Si CCD array camera. The current camera uses a 2184 x 1472 pixel array (15 mm x 10 mm), with a pixel size of 6.8 x 6.8 μm^2 and can be used for transport imaging for wavelengths from ~ 350 to 1100 nm. Initial image processing is performed using MicroCCD, a software program provided with the CCD camera. Although further image and data processing are often required for individual investigations, we benefit from excellent existing image acquisition and processing capabilities, often developed to support astronomical communities using similar cameras for low light imaging.

The optical microscope insert is a basic two lens system (objective and eyepiece) modified to allow for passage of an incident electron beam. The considerations, as with any optical microscope, are resolution and magnification. Estimating the resolution for incoherent emission as

$$\Delta y \sim \frac{0.61\lambda}{NA} \tag{17}$$

(where Δy is the spatial resolution, λ is the wavelength and NA is the numerical aperture (set here at 0.95 max)), we find $\Delta y = 0.56$ μm for $\lambda = 870$ nm (e.g., room temperature emission from GaAs) and $\Delta y = 0.22$ μm for $\lambda = 350$ nm (e.g., emission from GaN). The current magnification of the optical system is ~ 20x, i.e., a 5 x 5 μm^2 area scanned by the e beam creates a 100 x 100 μm^2 area on the CCD area. As mentioned, pixel dimensions are 6.8 μm, so the resultant effective scale for the final image is ~0.4 μm/pixel, comparable to the resolution limit for red/near IR light. In order to select photon emission from specific regions within the sample, appropriate combinations of bandpass filters are placed within the optical path for wavelength selection. The filters are used to eliminate, for example, substrate luminescence or to select the transport of interest in a multilayer sample.

While the optical resolution limit is the fundamental mechanical limit of the luminescence collection, there exists a further analytical bound on the extraction of transport properties related to the data extraction method.

C. DATA EXTRACTION

As discussed previously, the transport property information is contained in the distribution of minority carriers at steady state. This distribution is directly linked to the resulting photon distribution as captured in an image by our device. Figure 5 shows one such image.

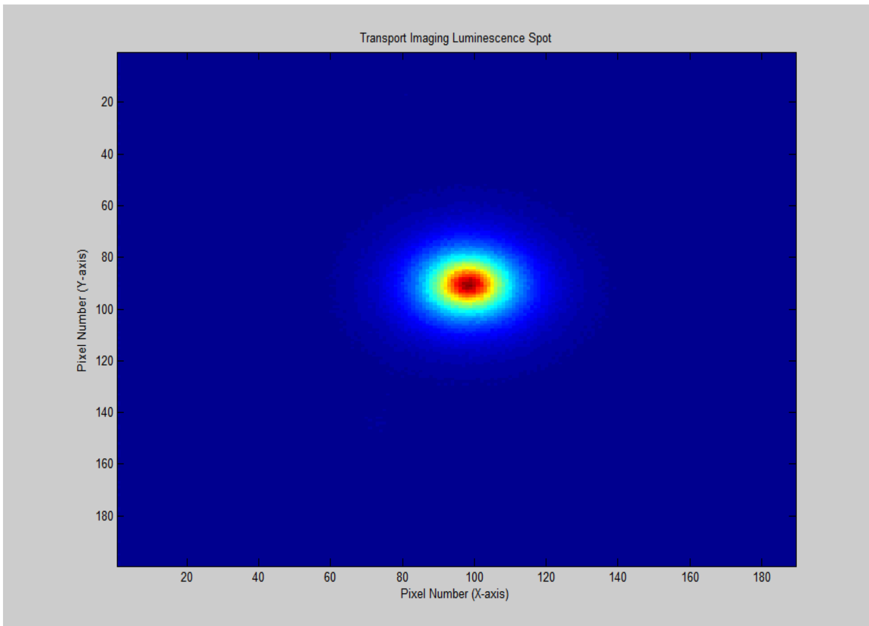

Figure 5. CCD image of Experimental Sample

The data underlying this image is a 2x2 matrix whose indices correspond to pixel number. The values entered in each element (0-10,000) of this matrix are the raw intensity of the photon emission collected by the CCD. In order to study the full extent of the distribution of minority carriers with greatest resolution, we extract line segments that cross the peak intensity point of the image. Though various methods may be employed to select these data sets, in this work that extraction was conducted via an algorithm written in MATLAB code (See appendix A.1- “imagedatamanipulator.m”). Once a line segment is extracted, it must be parameterized and fitted to the model equation developed in Chapter II. This fitting can be accomplished via two methods with varying degrees of flexibility and resolution.

1. Slope Analysis Estimation

By assuming that the argument of the Bessel function is large compared with 1 we can assume the distribution approximates a negative exponential.

With r>>L$_d$: $K_o(\frac{r}{L_d}) \rightarrow e^{\frac{-r}{L_d}}$

so that the slope of this line segment plotted on a semilog plot would be $m = \frac{-1}{L_d} = -\sqrt{\frac{e}{\mu\tau kT}}$ where

m is the slope and $r = \sqrt{x^2 + y^2}$, and all other terms are as defined in Chapter II. Figure 6 shows a semilog plot of a line segment extracted from the image of Figure 5.

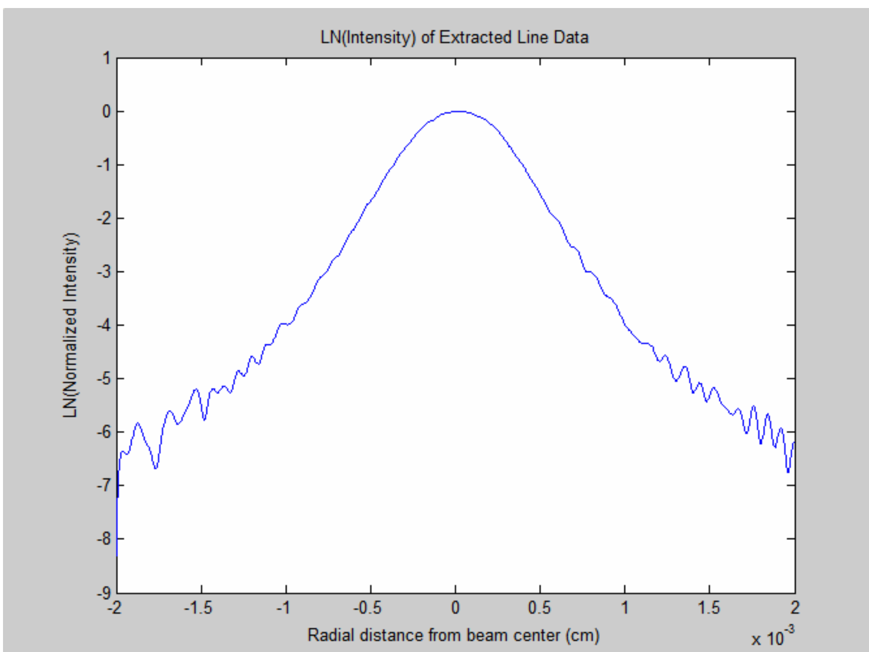

Figure 6. Semilog plot of extracted line of luminescence from Data Image of Figure 5.

Figure 7 shows the results of the slope analysis as calculated by the “Slope2.m” algorithm of Appendix A.3.

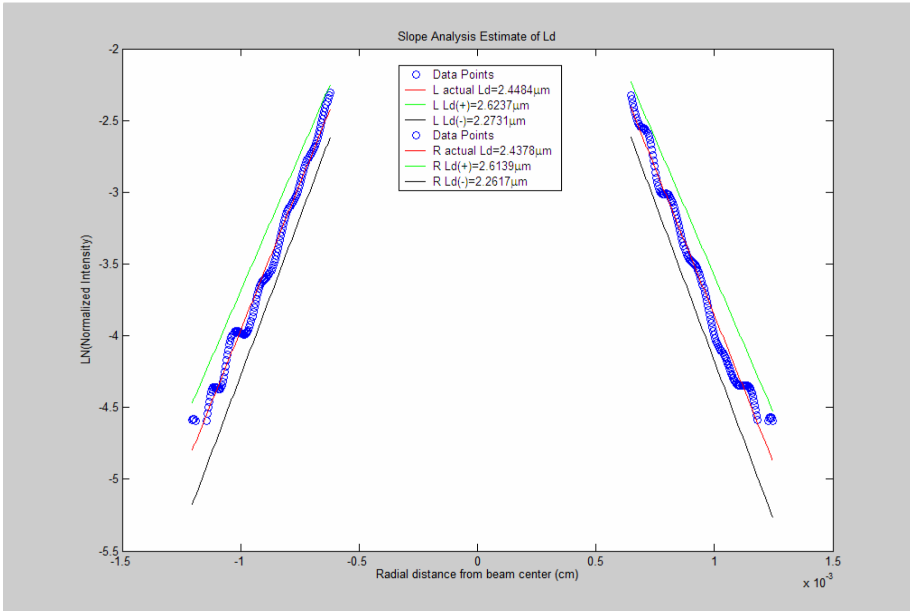

Figure 7. Slope Analysis for Experimental Sample

The error bars here are derived from the slope calculation of the distribution when the maximum possible mechanical error limits ($\pm 0.4\mu m$) are assumed for the first and last points in the data sample. This error analysis is utilized instead of a standard deviation of data points from the linear regression due to its physical nature. It provides an intuitive link between the analytical assessment and the mechanical limits of our apparatus.

The benefits of the slope analysis technique lie in its direct extraction of transport properties from an image with limited fitting or data manipulation. Depending on signal to noise ratio and sample luminosity it can provide knowledge of a material’s diffusion length over a roughly $3\mu m^2$ area. This material property resolution is limited by the optical resolution of the system (pixel width) in the $\hat{\phi}$

direction, equal to $0.4\mu m$, and the number of pixels required to conduct the linear regression analysis in the $\hat{r}$ direction. Figure 8 shows a pictorial of resolution dependence on data sample size and selection. The resolution listed in the figure follows from Figures 4-6.

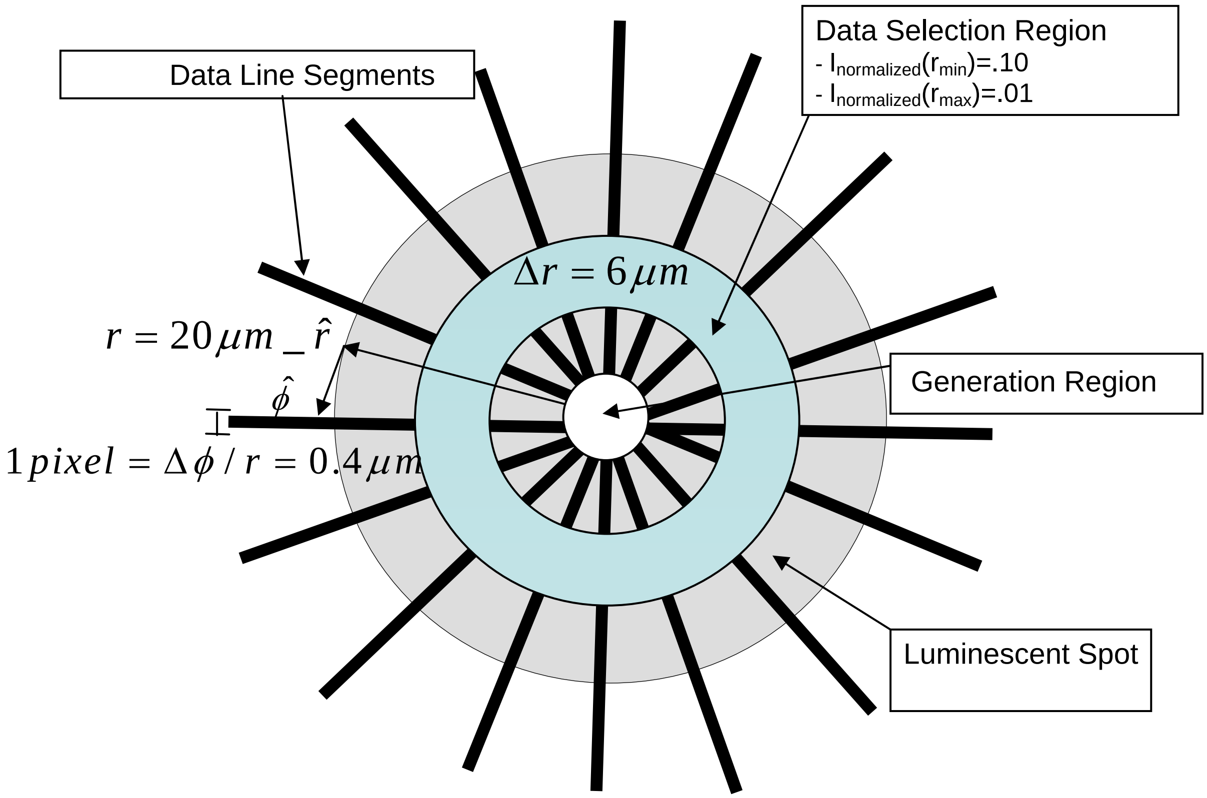

Figure 8. Slope Analysis resolution

So in this case, the sample resolution of transport properties is averaged over an area of $0.4\mu m$ x $6\mu m$ or $2.4\mu m^2$.

As mentioned, the sample size and region selection is a function of the interplay between signal to noise ratio, error analysis and the large r limit. Lower error estimations require a larger number of data points, while for most samples, noise limitations drive our outer limit below the ideal r/L_d>>1 limit. In work done by M. Talmadge of Fairfield University, Fairfield CT, it has been shown that when $r>9L_d$ the extracted -1/m is within 95% of the actual L_d. Figure 9 shows the trend of predicted L_d vs. actual L_d as a function of r/L_d[14].

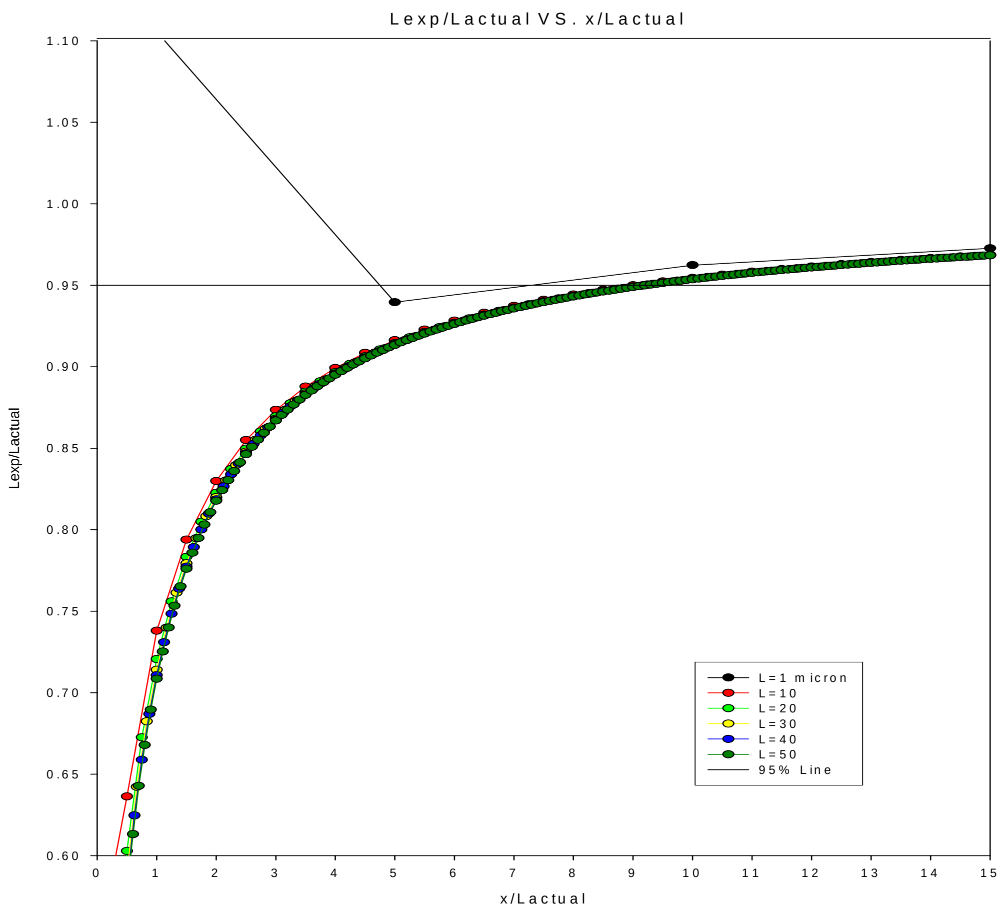

Figure 9. Slope Method Assumption Dependence on large Bessel Function argument

However, when L_d is not known it is more difficult to determine this confidence factor. Work is currently being done to perfect a second derivative analysis to determine this confidence factor without *a priori* knowledge of the actual L_d. Additionally, when our samples are of low luminosity and have short diffusion lengths the collected photon emission does not possess the required extent to allow data selection within reasonable limits of $r/L_d >> 1$. In this case a drift analysis is preferable however, it also possesses similar limitations.

2. Least Squares 2-Parameter Fit Analysis

By applying an iterative least squares analysis (See algorithm Appendix A.4) one can fit the model prediction from Equation (16) to the full distribution of the extracted line of data and determine the diffusion length of the minority carriers and the radius of 99% charge generation. This analysis technique provides an additional understanding of the generation region dimension and is unencumbered by the limitations of the $r/L_d >> 1$ limit. However, it increases the area of the sample used to extract a diffusion length – effectively reducing the resolution of the technique from $\approx 3\mu m^2$ to as large as $\approx 16\mu m^2$ for the same sample data from Figure 5. An example of a completed fit is shown in Figure 10, where n is defined as the radius which encompasses 99% of the carrier generation or $n = 2\sqrt{2}\sigma$.

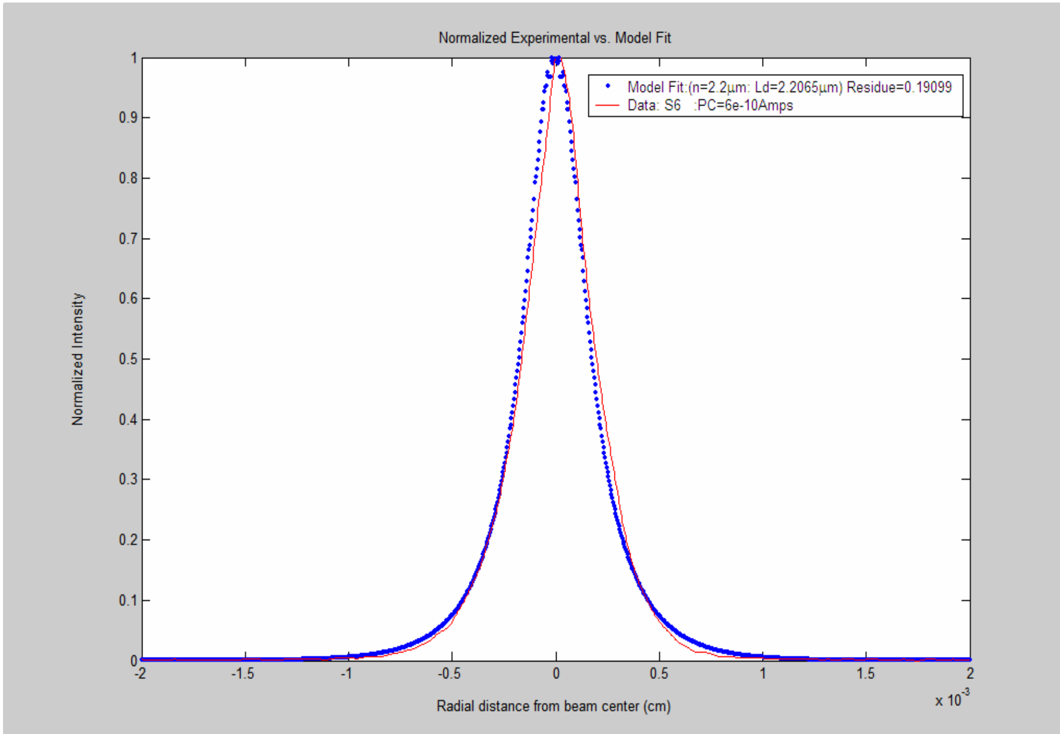

Figure 10. Least Squares Model Fit of Experimental Data

While the area over which the parameters are determined is larger, this technique benefits from the possibility of greater accuracy in determination of those parameters. Moreover, when the material studied has a diffusion length greater than our optical resolution, with appropriately taken data and reasonable signal to noise ratios we expect to extract diffusion lengths and generations region radii accurate to within $\pm 0.1\mu m$. As mentioned before, this method is not limited by the necessity to take data far from the generation source, which is difficult for materials of low luminescence. However, there are inherent limits to the materials and conditions which can be treated with this analysis.

THIS PAGE INTENTIONALLY LEFT BLANK

IV. TRANSPORT IMAGING PREDICTIONS AND LIMITATIONS

A. ERROR ESTIMATION FOR CURVE FITTING ALGORITHM

Apart from noise and resolution limits, there are two primary sources of error in this technique; 1) the fit of the model data to the experimental data, and 2) the assumptions that underlie our mathematical model. We can treat the quality of the model fit through the calculation of a root mean square error (RMSE).

The residue listed in the legend in each figure is the sum of the least squares difference used to select the most appropriate parameter fit. From this residue one can calculate the RMSE of the fit, or

$RMSE = \left(\frac{\phi}{M}\right)^{\frac{1}{2}}$ where $\phi = residue = \sum_{i=1}^{M=1000}\left(I_{pred} - I_{data}\right)^2$ and M is the number of data points taken from the sample and used in the model calculation. This is a direct measure of the undetermined error of the fit to the distribution. Using this formulation we routinely achieve very favorable RMSEs ($\leq 10^{-2}$).

As was noted, our optical resolution is approximately $0.4\mu m$, which results in only 100 data points taken over the $40\mu m$ interval shown in the figure. In order to smooth the distribution, we use a spine interpolation technique to increase our data set by a factor of 10. For relatively well behaved distributions, which these are, this technique has been shown to not alter the predictions of the model, yet allows a much higher confidence in the curve fit.

Because the model distribution is generated by a numerical integration calculation of an integral expression and the parameters are themselves arguments of non-linear functions, it is not readily apparent how this RMSE correlates to error bars in the parameters themselves. This analysis can be done and is explained in many non-linear least squares fitting texts, but it is more physical to vary diffusion length and generation radius by a small amount and observe the resulting magnitude of the RMSE from our model fit. The next series of plots show this estimation.

In order to establish a base line algorithm precision we first produce a model output for parameter values $n = 3.0\mu m; L_d = 2.0\mu m$, then allow the least squares fitting routine to analyze that output and fit it with the appropriate parameters. When the integration step size is identical for the model produced output and the least squares fitting algorithm the residue is 0 as expected. This is shown in Figure 11.

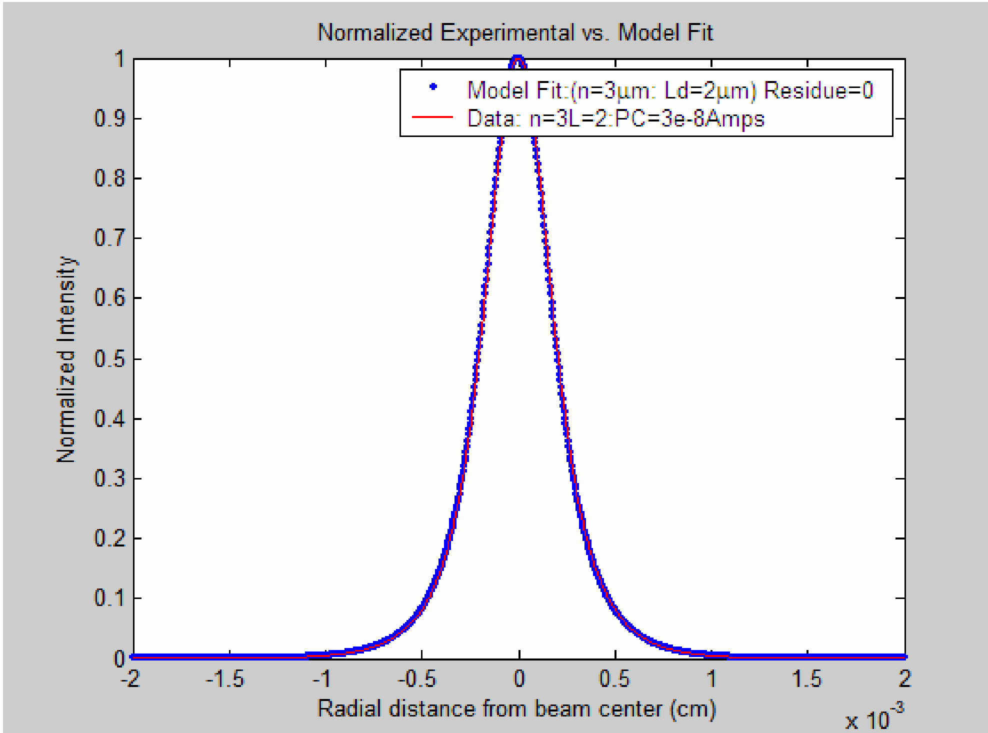

Figure 11. Baseline calculation error in Model Fit algorithm (no variation of integration step size)

A slightly more realistic assumption is that our numerical integration step size is on the order of 1000 times smaller than that of the experimentally captured distribution. Figure 12 shows the effect of a difference in integration step size of a factor of 1000 between the model produced curve and the least squares fitted curve.

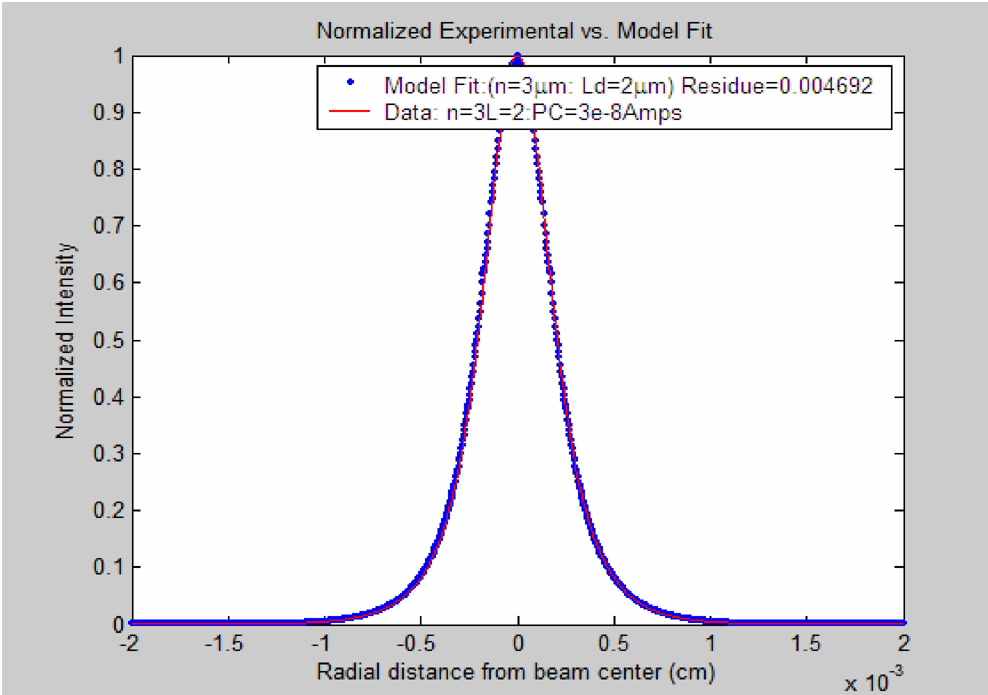

Figure 12. Baseline calculation error in Model Fit algorithm (variation of integration step)

The Residue of .004692 yields an RMSE of .0021 – an order of magnitude less than we typically see in our fitting to experimental data. We can, of course, reduce this step size but at the expense of integration time and given the very real effect of noise in our collected data, it is unrealistic to believe that we can achieve greater precision at room temperature through further reductions.

In order to see the effect of parameter errors on the Residue we again employ the algorithm to produce an ideal model distribution and fit it with our least squares routine. The figures that follow show forced errors in the model fit of the same ideal data set and the impact on the size of the residue. We vary diffusion length ($0.1\mu m$ and $0.2\mu m$) and generation region radius ($0.1\mu m$ and $0.01\mu m$) and calculate the RMSE in Table 2. It is noted that the RMSE value is approximately the same for equal variations in either parameter.

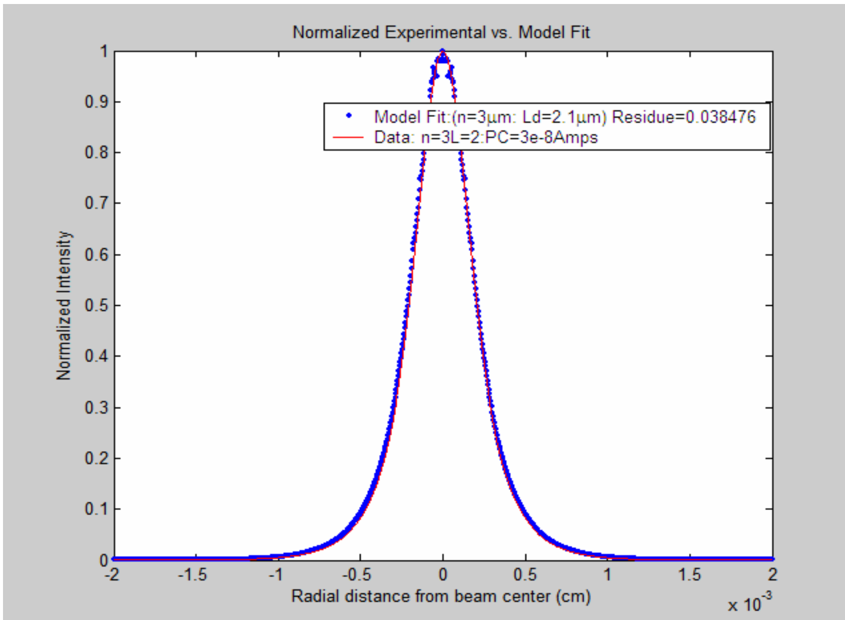

Figure 13. Error estimation for $0.1\mu m$ variation in Diffusion Length RMSE=$6.2x10^{-3}$

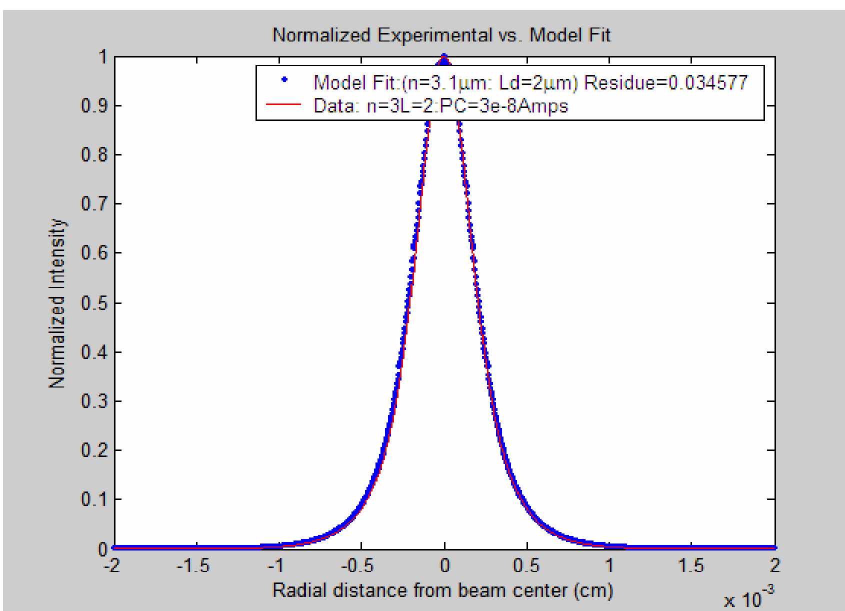

Figure 14. Error estimation for $0.1\mu m$ variation in Generation Region radius RMSE=$5.8x10^{-3}$

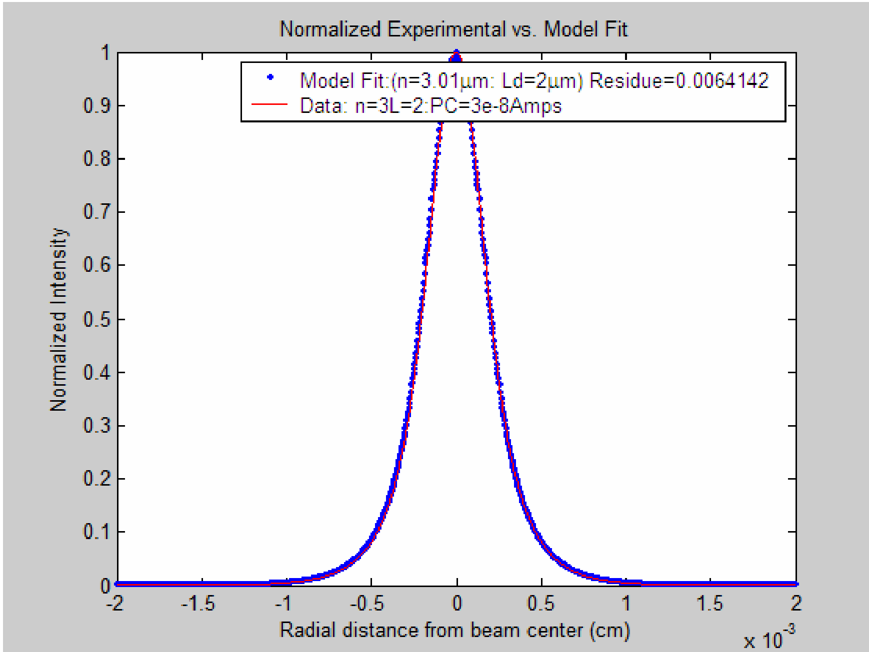

Figure 15. Error estimation for $0.01\mu m$ variation in Generation Region radius RMSE=$2.5x10^{-3}$

Another reference point for observed errors is shown in Figure 16.

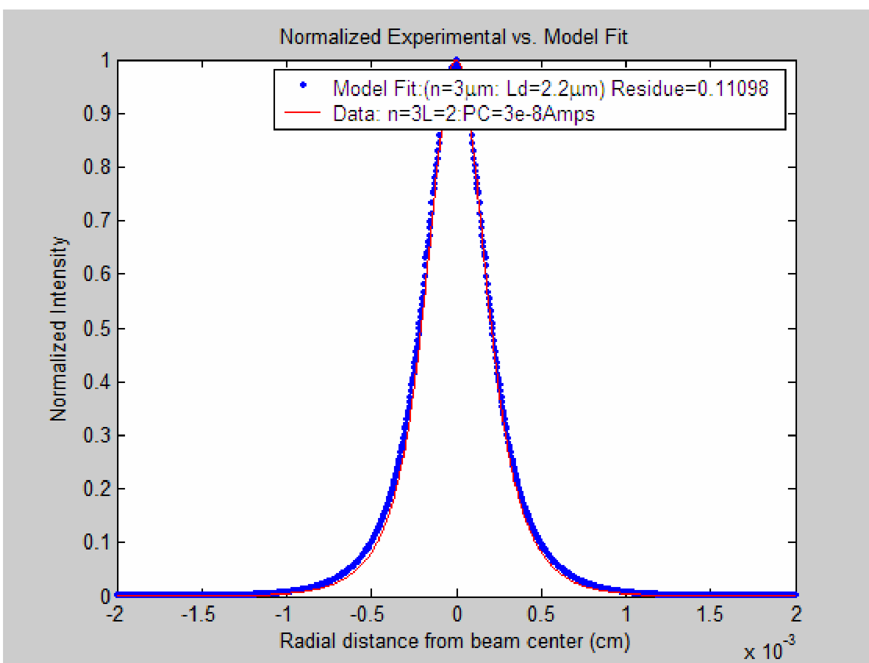

Figure 16. Error estimation for $0.2\mu m$ variation in Generation Region radius RMSE=$10.5x10^{-3}$

Residue	RMSE	L or n Variation
.0064	$2.5x10^{-3}$	$\pm 0.01 \mu m$
.0384	$6.2x10^{-3}$	$\pm 0.1 \mu m$
.1110	$10.5x10^{-3}$	$\pm 0.2 \mu m$
.4763	$21.8x10^{-3}$	$\pm 0.5 \mu m$
1.6853	$41.1x10^{-3}$	$\pm 1.0 \mu m$

Table 2. Tabulated Error Estimates for Curve Fits

B. LIMITS OF MODEL ASSUMPTIONS

A more fundamental error resides in the boundaries of where our model assumptions break down, or where other aspects of transport begin to play a more dominant role. There is much interesting science in this aspect of the analysis, and in fact, Chapter V will focus on the interplay of one such phenomenon, photon recycling, which at high doping levels begins to affect the luminescence distribution on a scale that demands special treatment.

1. Low Injection Assumption

An important limitation in our modeling is our assumption of low injection. As described in Chapter II.B. for these samples we are restricted to probe currents equal to or below $1x10^{-8} A$. Above this level of excitation we significantly alter the distribution of majority carriers in the vicinity of the generation region and the recombination is no longer appropriately described as proportional to the density of minority carriers alone. In order to probe this limit and to compare the slope analysis predictions with the model fit technique, we will observe a series of data taken from the same spatial location on an AlGaAs/GaAs heterostructure kept at a temperature of 4.7 K, and constant beam energy of 25 keV while the probe current was varied from $6x10^{-12} - 6x10^{-8} A$. Previous work within our lab has reported the effect of increasing SEM probe current on the size of the luminescent spot [17]. Here a series of images is presented corroborating this work and quantifying the increase in the standard deviation of the generation distribution. Figure 17 shows a schematic of the heterostructure as designed by Tom Boone at Hitachi Labs.

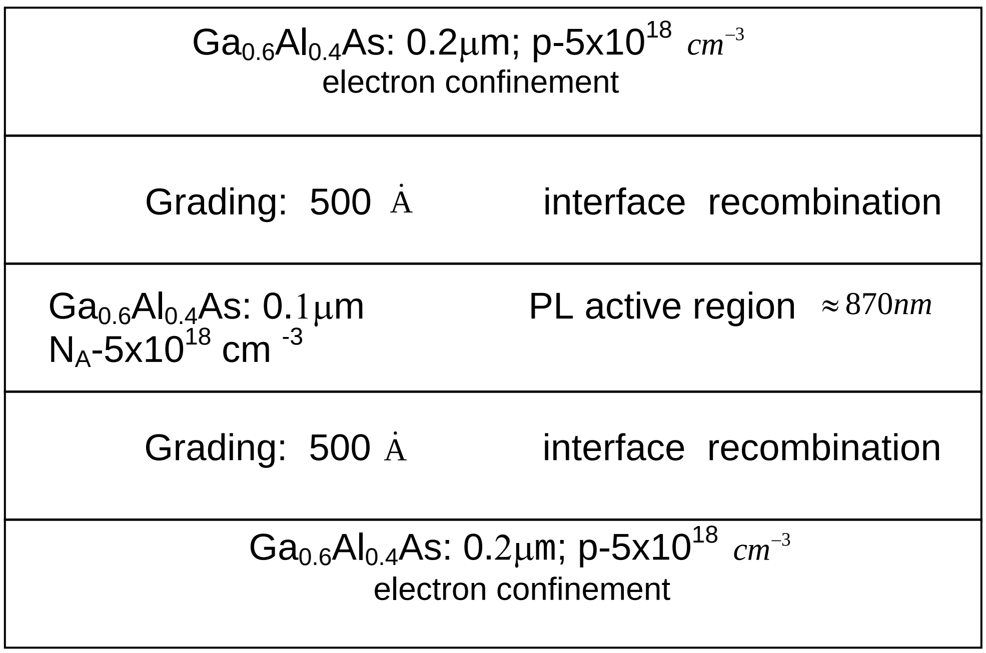

Figure 17. AlGaAs/GaAs Heterostructure design from Tom Boone Doctoral Dissertation [22]

The study of these materials at low temperatures allows a greater signal to noise ratio, which enables greater accuracy of the model fit. Previous work in our lab has shown that the minority carrier diffusion length in these materials is independent of sample temperature, and therefore we can use these measurements to establish a baseline of accuracy between the two techniques that should translate to higher temperatures [23]. Table 3 compiles the salient results from the analysis of this sample at 4.7 K.

Probe Current	L_d by Slope Analysis(μm)	L_d by Model Fit(μm)	$2\sqrt{2}\sigma$ Generation Region	RMSE of Model Fit
$6x10^{-12}A$	10 ± 8	3.9 ± 0.5	3.2 ± 0.5	$25x10^{-3}$
$6x10^{-11}A$	2.9 ± 0.2	3.7 ± 0.2	3.8 ± 0.2	$12x10^{-3}$
$6x10^{-10}A$	2.9 ± 0.2	4.1 ± 0.1	4.2 ± 0.1	$9x10^{-3}$
$6x10^{-9}A$	3.4 ± 0.2	4.4 ± 0.3	4.5 ± 0.3	$15x10^{-3}$
$6x10^{-8}A$	3.4 ± 0.2	4.7 ± 0.3	4.9 ± 0.3	$15x10^{-3}$

Table 3. Measurement Results for $0.1\mu m$ active layer, Boone Heterostructure #9

2. Slope Analysis Limitations and the Low Injection Limit

As can be seen from the tabulated values, increasing probe current tends to increase the effective radius of the generation region, as expected and reported previously in ref [17]. The diffusion length as measured by both techniques is relatively constant as a function of probe current below $6x10^{-8}A$ in accordance with our model assumptions. Also evident is the disparity between the slope analysis method and the model fit. This difference is expected and is related to the degree to which the slope analysis limiting assumption of large Bessel function argument is valid. That is, the slope analysis predictions assume that we are in a regime where the Bessel function argument $\frac{r}{L_d} >> 1$. In this case, measurements were taken over a distance of 7-14μm from the center point. Assuming an L_d actual of 4μm we can estimate the degree of disparity that should result by consulting Figure 9. Entering the X-axis with a value of $7/4$ or 2.5 we extract a Talmadge factor of 0.75, or we would expect that the slope analysis method would predict a value within 75% of the actual. This corresponds well to the ratio of the model fit prediction to slope analysis prediction 3μm/4μm – or 0.75. The lowest probe current shows the limits due to noise in this analysis. As expected, the slope analysis method will be impacted more greatly by poor signal to noise ratios because of its higher spatial resolution.

The figures that follow show the comparison between slope analysis plots and model fit plots. It is instructive to observe which portions of the model fits begin to deviate from the experimental data for higher probe currents. The trend away from low injection can be tracked by observing the deviation in the "shoulder" regions of the distributions as the probe current increases, (Figures 20,21, and 22.)

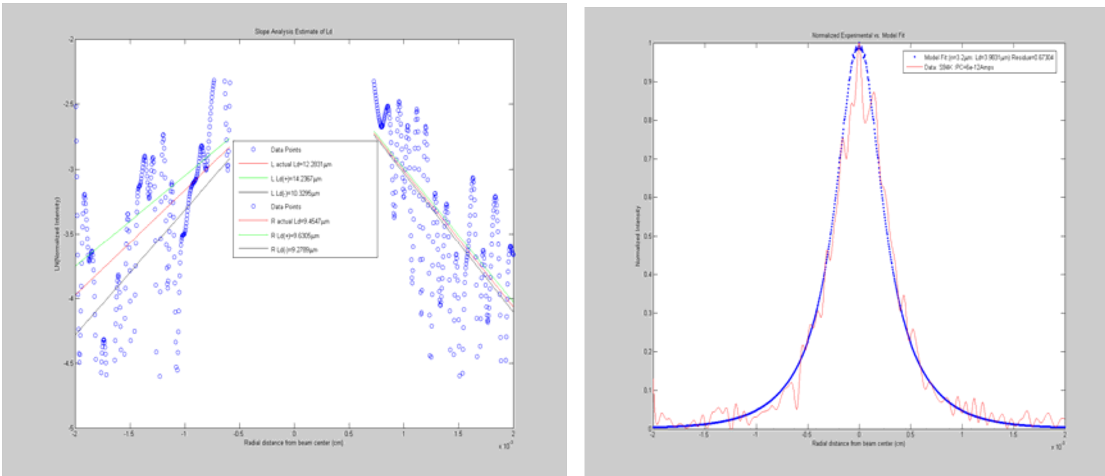

Figure 18. Slope and Model fit analysis plots for $6x10^{-12}A$ probe current (pertinent data tabulated in Table 3)

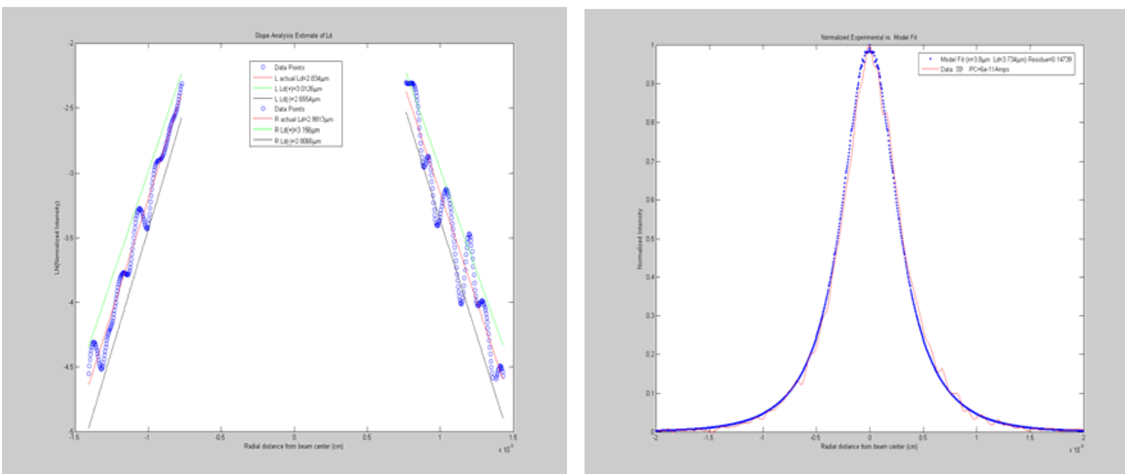

Figure 19. Slope and Model fit analysis plots for $6x10^{-11}A$ probe current (pertinent data tabulated in Table 3)

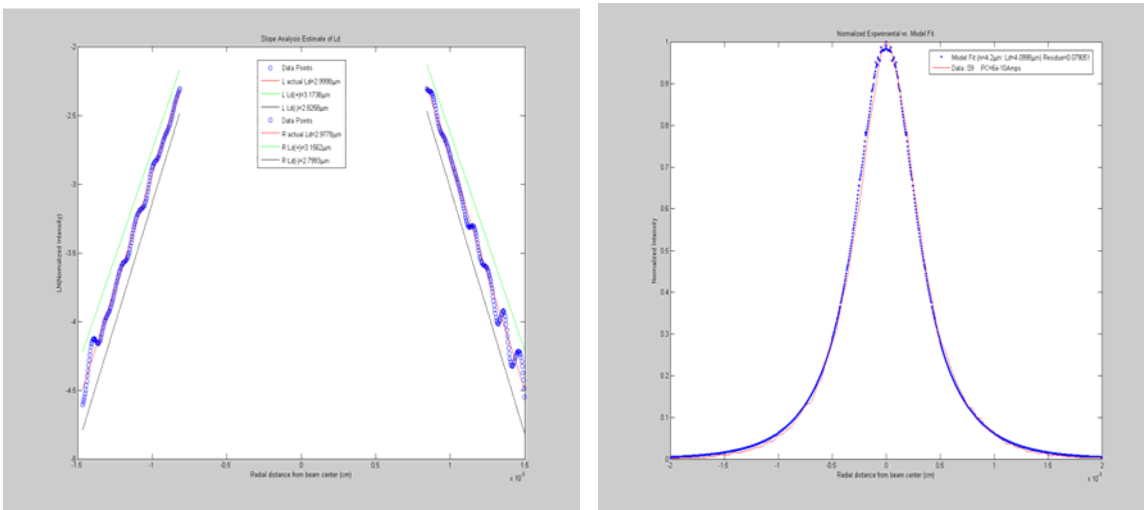

Figure 20. Slope and Model fit analysis plots for $6x10^{-10}A$ probe current (pertinent data tabulated in Table 3)

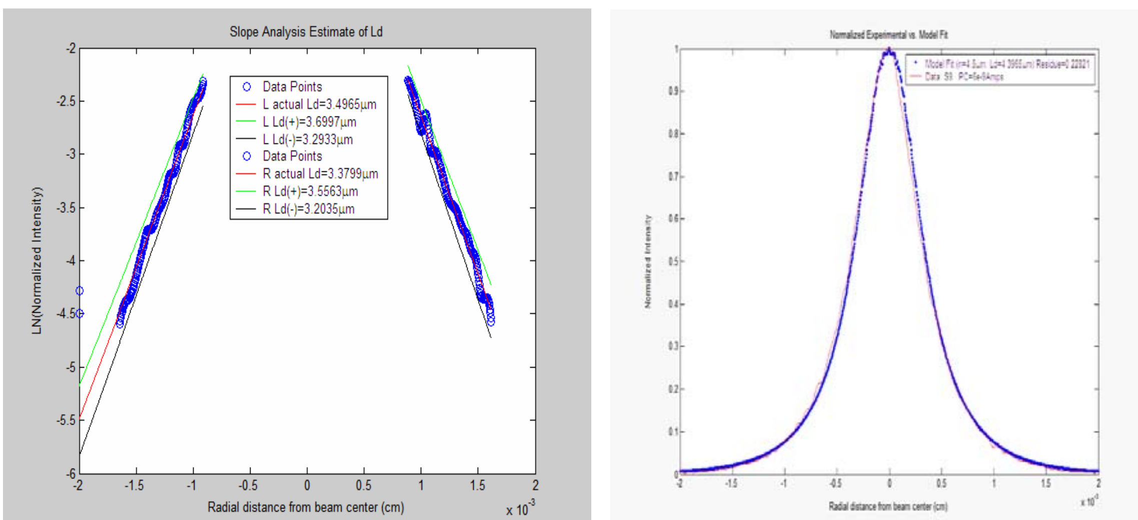

Figure 21. Slope and Model fit analysis plots for $6x10^{-9}A$ probe current (pertinent data tabulated in Table 3)

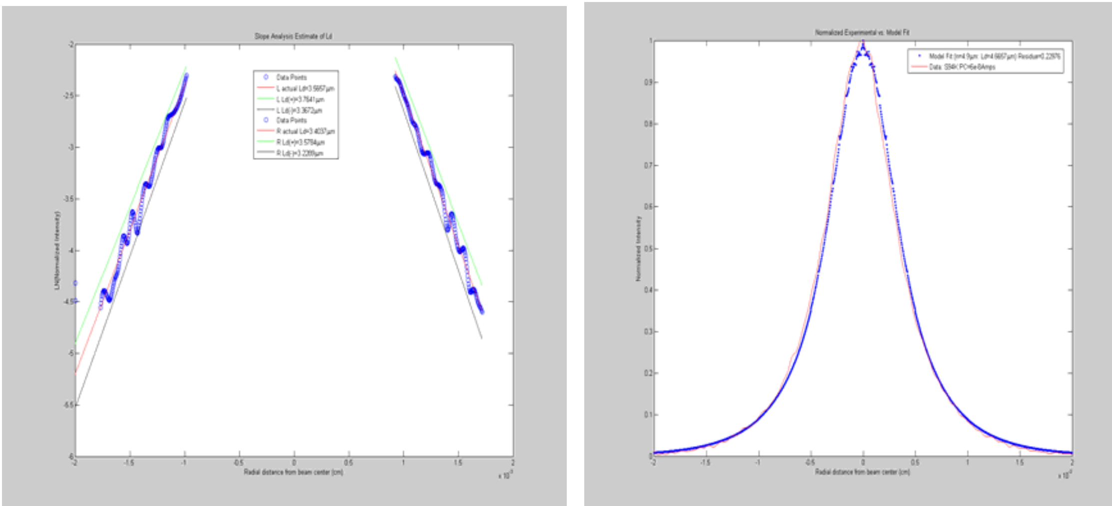

Figure 22. Slope and Model fit analysis plots for $6x10^{-8}A$ probe current (pertinent data tabulated in Table 3)

From Table 3 we can see that the balance between signal to noise, and model limitations place the best probe current for accurate measurement at $6x10^{-10}A$ for this sample.

3. Small Diffusion Length Limitations and the Role of the Generation Distribution

A more substantive measurement limitation for the heavily doped materials discussed in Chapter I is the relatively small diffusion lengths that accompany such large concentrations of acceptor dopants. While the literature predicts an increase in the minority electron mobility in GaAs doped with Be starting at $5x10^{-18}cm^{-3}$,[23] the lifetime continues to trend downward at a rate which overpowers the increase in mobility and causes diffusion lengths to continue to decrease. Just beyond this concentration the diffusion length drops below $1\mu m$, and we approach another limit of our technique. This limit is directly related to the generation region. In order to see how this limit arises, we again study our solution to the transport equation for a Gaussian generation distribution.

(16) $$n(x,y) = \frac{1}{2\pi L^2} \int_0^{2\sqrt{2}\sigma} K_o\left(\frac{\sqrt{S^2+4L^2}}{2L^2}\left|r-r'\right|\right) e^{\frac{S(x'-x)}{2L^2}} e^{\frac{-r'^2}{2\sigma^2}} dr'$$

Here the two terms which contribute to a zero E field (S=0) diffusion are the Bessel function and the Gaussian source function. As previously discussed, our use of the Bessel Equation comes from well-established differential equation theory for solving diffusion equations in 2D carrier transport and other disciplines governed by the Helmholtz Equation. The assumption of the Gaussian distribution to represent the carrier generation region within the sample is based upon the statistical interpretation of the electron-electron scattering and in limited cases is backed by empirical evidence [18],[20],[21].

More recently, work in our lab has shown that these distributions may not all fit the same mathematical dependence [19]. By assuming a standard Gaussian distribution, we may be neglecting effects of small deviations due to sample geometry, beam inhomogeneities, and possibly other effects that govern the sub-micrometer scale granularity of the minority carrier distribution. These inaccuracies in our model will become more prevalent when materials of small diffusion length are studied. Moreover, it is anticipated that when materials which have diffusion lengths on the order of our optical resolution are studied, it will become difficult to observe the effect of diffusion on the distribution. At this limit we may say that we are indeed observing the generation region itself. As we approach this limit, the accuracy of our representation of the interaction region will become increasingly important. Any deviation of the actual distribution from our Gaussian model will be reflected in some mixture of parameter adjustments, which will unrealistically be portrayed as diffusion length or sigma variation by the fitting algorithm.

In order to make a quantitative assessment of this limit we will demonstrate a limiting case. By producing a distribution data set defined as a pure Gaussian (n=$3.0\mu m$) and allowing the fitting algorithm to fit Equation (16) to it, we may see what a material with no diffusion and a perfect Gaussian generation distribution might look like. Figure 23 shows the slope analysis and model fit for this case and demonstrates that both methods inaccurately predict a diffusion length of $0.3\mu m$. As predicted, the model fit compromises the generation region radius of the distribution from its known value of $3.0\mu m$ in order to fit the data with a diffusion length that allows for the smallest residue permissible.

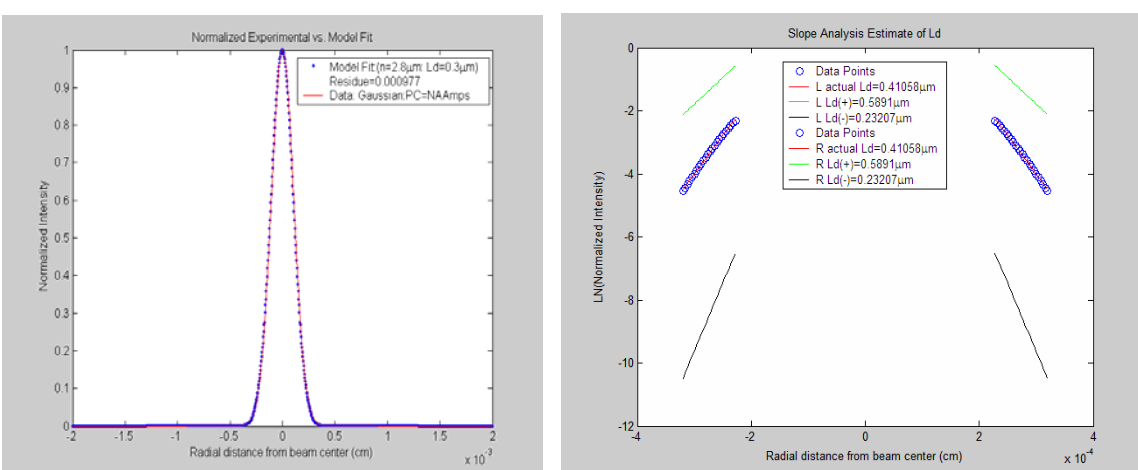

Figure 23. Pure Gaussian Distribution Model Fit

In other limiting cases where the modeled data set was produced with very small but non-zero diffusion lengths, the algorithm's accuracy was directly proportional to the step size, (analogous to pixel size) used in the creation of the data. This is consistent with our prediction that our CCD pixel size results in an effective lower limit of discernability 0.4μm for either parameter value. However, because the generation distribution radius does not approach this lower value, it is effectively only a limit for our determination of diffusion lengths. Compounding this lower limit is any inaccuracy in our assumption of generation region form, which will tend to distort both σ and L_d. As we approach the regime where the form of the generation distribution contributes more than does diffusion to the shape of the overall distribution we expect this limitation to have a larger and larger effect. Moreover, the 0.4μm error suggested above is only accurate when you assume a perfect Gaussian generation region. Any deviation of the generation region from the ideal will tend to increase our baseline error.

In reference [19] Luber discusses the use of this same Transport Imaging technique as a means to more accurately determine the interaction region distribution for materials of interest. While a full quantitative method has not been developed, it is seen as a key step toward the study of very small diffusion length materials ($L_d \leq 1.0\mu m$).

V. STUDY OF HEAVILY DOPED HETEROSTRUCTURES

A. MOTIVATION

As discussed in Chapter I, faster switching transistors are of prime importance to military applications. The devices that are currently under development to handle this task, in commercial applications as well as military, are HBTs. The key device parameter for increasing speed and efficiency is the base layer transit time. Many engineering design approaches are used to decrease the time it takes electrons to flow across the base layer, but the efficient use of these techniques is dependent upon the accurate knowledge of the transport properties - minority electron diffusion length, lifetime, and mobility.

A mathematical description of the base transit time reveals the importance of low dimension construction as well.

$$\tau_B = \frac{W^2}{2D_p} \tag{18}$$

where τ_B is the base transit time, W is the base width, and,

$$D_p = \mu_p kT / e \tag{19}$$

is the minority carrier diffusion coefficient as defined by the Einstein equation where μ_p is the minority carrier mobility, e the charge on an electron, k Boltzman's constant, and T is the temperature in Kelvins [1].

The appearance of the base width as a squared term dominates the trend of transit time, but with decreased base width comes the problem of emitter-collector current leakage. Here, increased dopant concentrations aid the reduction of the base width by providing an impediment to this current leakage, however, classical analysis predicts that increased doping has a negative effect on τ_B through its reduction of μ_p and therefore D_p [1]. Classically, one would predict a practical limit to the concentration of dopants that can be used as the competing effects of reduced D_p and decreased W interact. However, a more detailed analysis reveals a more complex picture.

B. QUANTUM MECHANICAL PREDICTIONS

An observation of nonconventional electron current density in an GaAs/AlGaAs N-p-n HBT with Be base doping of $6x10^{18}cm^{-3}$ led Lyon and Casey to believe that some other transport mechanism was at play. They observed a collector-emitter current density that exceeded conventional predictions by four times [29]. More recently, material growth techniques have improved and base layers are being produced with graded doping schemes in the low $10^{20}cm^{-3}$ [5]. At these levels the assumptions of the Boltzman distribution and classical carrier scattering descriptions may not be sufficient to explain carrier transport. In work done by Bennett and Lowney employing a first principles quantum mechanical analysis of scattering mechanisms in heavily doped GaAs, it is predicted that a local minima exists for electron mobility in the $5x10^{-18}cm^{-3}$ regime. This analysis includes all the important scattering mechanisms for the low-field mobilities: acoustic phonon, polar optic phonon, piezoelectric, ionized impurity, carrier-carrier, alloy, and plasmon scattering. The upturn in the mobility results from the dependence of these scattering mechanisms on the dopant and carrier density. As the dopant density increases the average distance between holes decreases. This screening radius then determines the upper frequency that may be supported for the vibrational modes set up in the plasma of majority carrier holes, plasmon cutoff frequency (PCF). As the PCF increases, the scattering interaction probability between minority carrier electrons and plasmons decreases. Additionally, as the free hole concentration increases the lower energy bands fill, and Pauli Exclusion Principle screening becomes important. The number of majority carrier/minority carrier scattering events is reduced because the holes are precluded from changing their energy level and therefore can not interact [23].

These results have been difficult to reinforce experimentally and limited direct evidence exists to support them [25-28]. A method to observe this effect in a non-contact manner which requires little sample preparation and is non-invasive would add to existing device diagnostics techniques. Transport Imaging provides such a solution.

C. EXPERIMENTAL RESULTS

In order to observe this increasing mobility trend a series of Be doped heterostructures was studied. Figure 24 shows the design of the studied structures.

$Ga_{0.6}Al_{0.4}As$: 0.2μm; p-5x10^{18} cm^{-3} electron confinement	
Grading: 500 Å	interface recombination
$Ga_{0.6}Al_{0.4}As$: 1.0μm; N_A-3x10^{18} - 1x10^{20} cm^{-3}	PL active region peak emission $\approx 870nm$
Grading: 500 Å	interface recombination
$Ga_{0.6}Al_{0.4}As$: 0.2μm; p-5x10^{18} cm^{-3} electron confinement	

Figure 24. Heterostructure design as grown by Tom Boone, (From Ref. [22])

The Transport Imaging technique was applied to seven samples of differing active layer doping and the diffusion length of the samples was extracted using both the slope analysis method and the two parameter fit. Data were taken at multiple locations on each sample, on different days and under varying beam energy and probe currents. Though some variation of parameter value with location was noted, overall the samples can be considered to be very homogeneous, and these results to be representative of the average properties. In order to test the predictions of Dr. Bennett, we required lifetime (τ) values with which we could extract mobility (μ) values from our diffusion length measurements through the relationship of Equations (3) and (18). We coupled independent measurements of the sample lifetimes with values provided by the grower, Dr. Boone. In both cases the measurements were made by time resolved photo-luminescence techniques. Table 4 tabulates the initial measured values for these samples. The lifetimes marked with an asterisk were measured in 2003-2004 by Yale University and were not corroborated by our independent and more accurate TRPL confirmation. Comparisons between the Yale reported lifetimes and our TRPL measurements for the other samples showed a 10% overestimation in the samples of with Na>x10^{19} cm^{-3}.

Sample	**Doping[cm^{-3}]**	**τ [ps]**	**L_d [μm]**	$\mu \left[\frac{cm^2}{V \cdot s}\right]$
A2	$2.75x10^{18}$	2050 *	$3.6 \pm .1$	2500 ± 140
B7	$3.75x10^{18}$	900	$2.3 \pm .1$	2350 ± 200
C9	$5x10^{18} \pm 3x10^{18}$	4800	$4.1 \pm .1$	1333 ± 68
D6	$3.5x10^{19}$	95	$1.6 \pm .2$	10800 ± 2800
E3	$4.0x10^{19}$	140 *	$1.8 \pm .15$	9200 ± 1600
F4	$6x10^{19}$	116 *	$1.9 \pm .1$	12400 ± 1300
G8	$1.0x10^{20} \pm .1x10^{20}$	11	$1.7 \pm .2$	101000 ± 25300

Table 4. Initial results of AlGaAs/GaAs heterostructure study

1. Initial Observations

The result for sample C9 is the only sample that is completely consistent with Dr. Bennett’s predictions. It is also the sample tested in Chapter III, and possesses an active layer dimension 10 times thinner than the other samples. Samples B2 and C7 are consistent with Bennett’s trend of decreasing mobility toward the inflection point at a concentration of $5.0x10^{18}cm^{-3}$ though offset by approximately $1000\frac{cm^2}{V \cdot s}$. Other reported data for mobilities in this range of doping concentrations also show elevated values compared with Bennett's predictions [24]. However, the mobilities for samples D-G are unrealistic, even if the trend of increasing mobility is evident.

The consistent positive offset of these values suggests a systemic error or effect that is operational in the $>10^{19}cm^{-3}$ samples. We propose two reasons for these offsets and apply appropriate offsets to account for them.

2. Generation Region Discrepancies

As mentioned in paragraph B, we expect that as we approach the regime where the generation region contributes more and more to the shape of the extracted curve, we will be subject to limitations due to inaccurate assumptions about the generation region. By studying the curve fits in the higher doped samples we can gain some intuition about where this limit may be. The figures that follow (Fig. 25-28) are the best residue curve fit achieved for each of the samples.

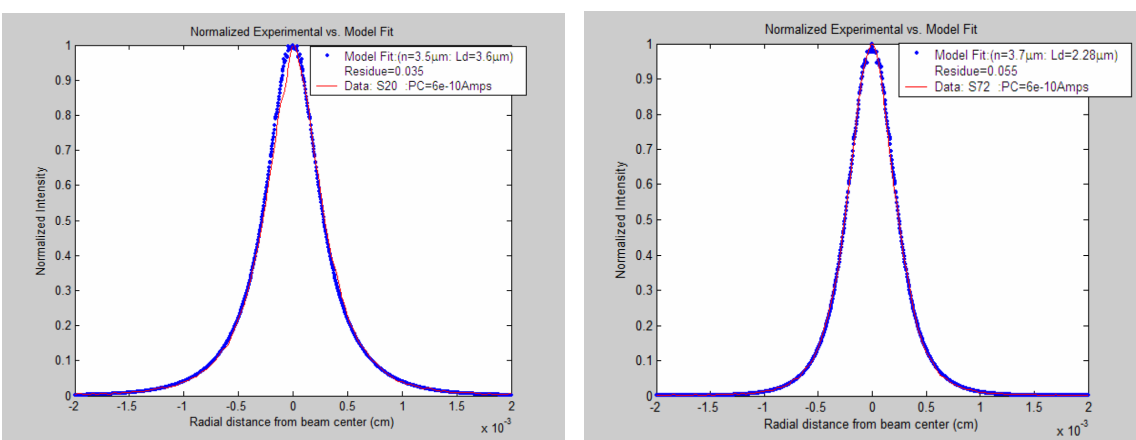

Figure 25. Samples A2 and B7 best fit 2-parameter fit extractions

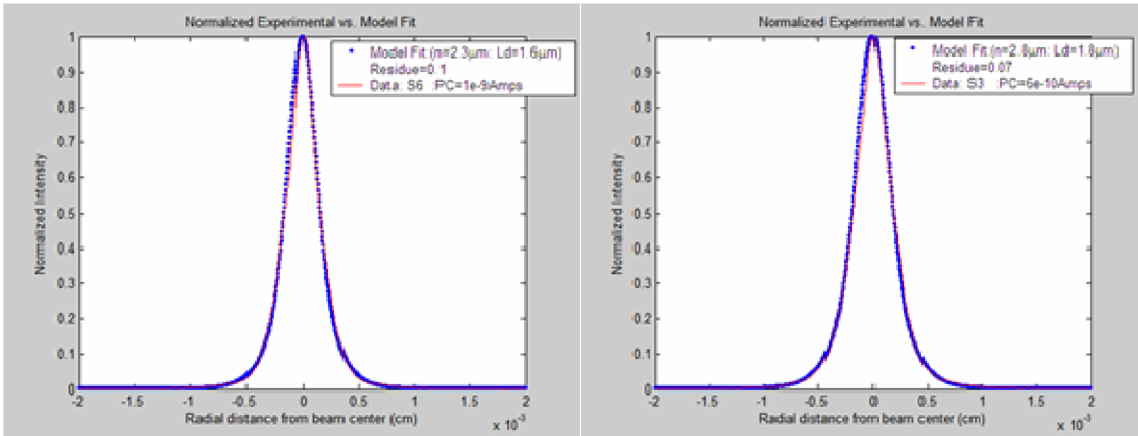

Figure 26. Samples D6 and E3 best fit 2-parameter fit extractions

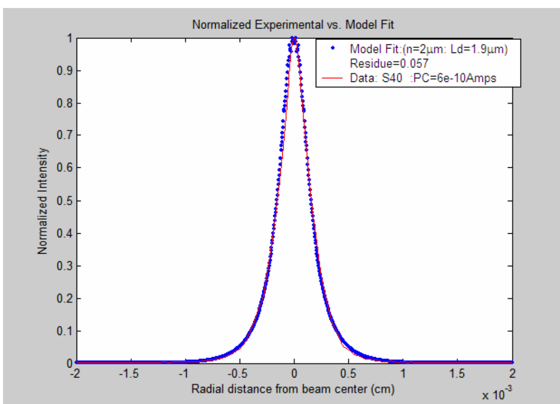

Figure 27. Sample F4 best fit 2-parameter fit extraction

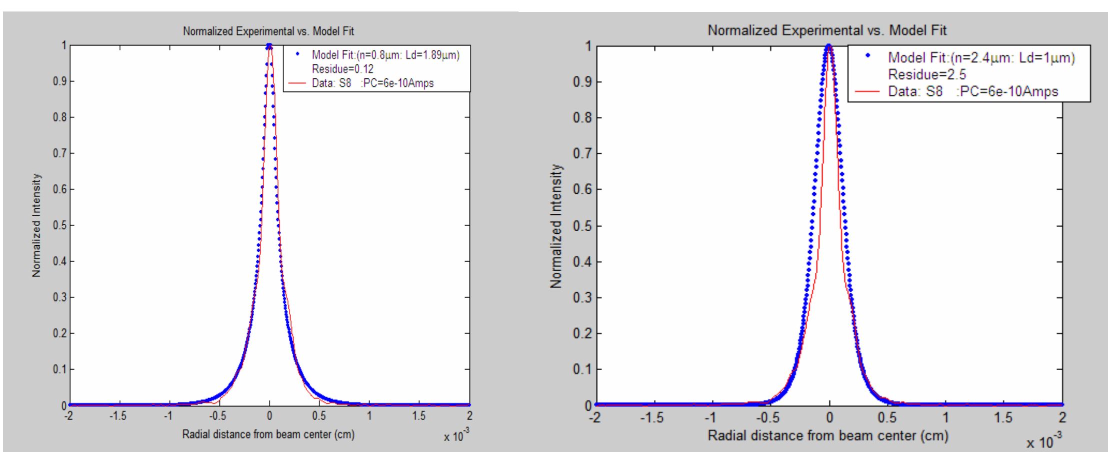

Figure 28. Sample G8 best fit (a) algorithm run, (b) Assumed reasonable generation region with algorithm fitted diffusion length

The generation region radius has been shown to increase with probe current and with beam energy, but here we see a decrease in the generation region as a function of dopant concentration. Also noted is the tendency of the model fit to depart from the data set in the region of the shoulders of the curves near the base of the distribution. This effectively causes an overestimation of the diffusion lengths as predicted in Section B. Finally, we can surmise that in samples D-G we are in the realm where the diffusion lengths are on the order of the generation region radius, or less, and approaching a fundamental limit of our assumptions. If we assume that the produced error is on the order of that demonstrated with the pure Gaussian from Chapter IV, Section C. we would expect an overestimation of the diffusion length by 0.4μm.

3. Photon Recycling (PR)

Another important and well-documented effect that must be considered is that of Photon Recycling. The literature is replete with documentation of this phenomenon that affects diffusion coefficients and observed lifetimes in bulk GaAs that begins to act in this doping regime [30-32]. The effect is treated in different manners, but consistently results in correction terms being used to adjust the observed diffusion coefficient and total lifetime. Renaud treats the effect as an addition to the generation function in the continuity equation (our Equation (10)). He defines the photon recycling generation function: [30]

$$G_{PR} = \frac{\alpha_i}{2\tau_r} \int_0^w K(x,x')\Delta n(x',t)dx' \qquad (20)$$

This represents the excitation in the sample with thickness w and average absorption coefficient α, taking into account the spectral density of the light. τ_r is the radiative lifetime related to the lifetime we measure with TRPL by

$$\frac{1}{\tau} = \frac{1}{\tau_r} + \frac{1}{\tau_{nr}} \tag{21}$$

where τ_{nr} is the non-radiative lifetime. The real perturbation comes from the calculation of K(x,x'), which is related as a series of exponential integral functions [30]. The minority carrier distribution is then expanded in a series expansion over the photon recycling source region and the continuity equation is now adjusted with each term possessing a PR pertubation factor T_n, where:

$$T_n = \frac{1}{n!}\frac{\alpha_i}{\tau_r}\int_{-x}^{w-x} K(x, x+u)u^n du \tag{22}$$

Because K is principally a function of exponential integral functions and converges quickly to zero with increasing n, they can be represented by the spatial average value $\langle T_n \rangle$. Appendix B lists the first two non-zero terms of this series: $\langle T_0 \rangle and \langle T_2 \rangle$ in their full mathematical form, as well as the exponential integral function. The resulting continuity equation is a modification of our Equation (4.5):

$$0 = G_n - \left(\frac{1}{\tau_n} - \langle T_0 \rangle\right)n - \mu_n E\frac{dn}{dx} + \left(\frac{L^2}{\tau_n} + \langle T_2 \rangle\right)\vec{\nabla}^2 n \tag{23}$$

Renaud demonstrates good agreement between his corrective terms and behavior of GaAs LEDs and photovoltaic cells, and calls for more study on small thickness samples. Badescu states that while photon recycling is most apparent in bulk samples, there is a more pronounced effect in samples where the absorption length $L_\alpha \equiv \frac{1}{\alpha}$ exceeds the diffusion length, even for thinner samples (<1μm) [31].

If we add a column to Table 4 and populate it with the absorption coefficient α (taken from [33]) and the absorption length for each sample we see a correlation between the departure from predicted values of mobility and the breakpoint where absorption length exceeds diffusion length.

Sample	**Doping**[cm^{-3}]	τ [ps]	**L_d** [μm]	α [μm^{-1}]	**L_α** [μm]	$\mu \left[\frac{cm^2}{V \cdot s}\right]$
A2	$2.75x10^{18}$	2050 *	$3.6 \pm .1$	5000	2.0	2500 ± 140
B7	$3.75x10^{18}$	900	$2.3 \pm .1$	4500	2.2	2350 ± 200
C9	$5x10^{18} \pm 3x10^{18}$	4800	$4.1 \pm .1$	4000	2.5	1333 ± 68
D6	$3.5x10^{19}$	95	$1.6 \pm .2$	3500	2.85	10800 ± 2800
E3	$4.0x10^{19}$	140 *	$1.8 \pm .15$	3400	2.94	9200 ± 1600
F4	$6x10^{19}$	116 *	$1.9 \pm .1$	3000	3.3	12400 ± 1300
G8	$1.0x10^{20} \pm .1x10^{20}$	11	$1.7 \pm .2$	2300	4.3	101000 ± 25300

Table 5. HS data table with absorption length comparison

C. CORRECTIONS FOR OPERATIVE EFFECTS AND DISCUSSED LIMITATIONS

The photon recycling effect is dependent upon the number of photons generated, the rate at which they reabsorb, but also on the rate at which they can escape the active layer before creating additional electron-hole pairs. The first dependencies we have previously described, but now we must look at the index of refraction of our samples and the corresponding critical angle of total internal reflection.

In 1976 Asbeck reported the critical angle for GaAs/AlGaAs interfaces as a function of various Al concentrations [35]. Interpolating from his graphs and confirming with Snell's Law, we arrive at a critical angle for the active GaAs layer of 69.6^o The index of refraction varies with dopant density as well, but because the differences are small between AlGaAs and GaAs we can use the value for GaAs as 3.59 and for 40% Al concentration in AlGaAs n=3.36. Using these values to calculate the Reflectance; [36]

(23) $$R = \left(\frac{1-n}{1+n}\right)^2$$

For $n = \frac{n_{AlGaAs}}{n_{GaAs}} = \frac{3.36}{3.59} = .935$ and therefore $R = 0.1\%$, or when light strikes the interface at an angle less than the critical angle, 99.9% will transmit through to the AlGaAs layer.

Also required is the radiative lifetime. From [32] we can define:

(24) $$\tau_r = \frac{1}{2x10^{-10} \cdot N_A}[s]$$

Now to calculate the correction factors and apply them to our experimental results for the samples in Tables 3 and 4 we employ the MATHCAD routine of Appendix B.1. The detailed calculation sheets are in Appendix B.x and the overall results are tabulated below in Table 6.

Sample	**Doping** [cm^{-3}]	τ [ps]	L_d** [μm]	$\mu \left[\frac{cm^2}{V \cdot s}\right]$	τ_{PR} [ps]	L_{dPR} [μm]	$\mu_{PR} \left[\frac{cm^2}{V \cdot s}\right]$
A2	$2.75x10^{18}$	2050 *	$3.6 \pm .1$	2500 ± 140	NC	NC	NC
B7	$3.75x10^{18}$	900	$2.3 \pm .1$	2350 ± 200	NC	NC	NC
C9	$5x10^{18} \pm 3x10^{18}$	4800	$4.1 \pm .1$	1333 ± 68	NC	NC	NC
D6	$3.5x10^{19}$	95	$1.2 \pm .2$	6000 ± 2000	69	$1.0 \pm .2$	6000 ± 2000
E3	$4.0x10^{19}$	140 *	$1.4 \pm .15$	5600 ± 1300	85 *	$1.1 \pm .15$	5500 ± 1600
F4	$6x10^{19}$	116 *	$1.5 \pm .1$	7800 ± 1000	66 *	$1.0 \pm .1$	7600 ± 1300
G8	$1.0x10^{20} \pm .1x10^{20}$	11	$1.0 \pm .2$	59000 ± 20000	9	$0.9 \pm .2$	36000 ± 15300

Table 6. Tabulated Parameters corrected for Generation Region error(**) and Photon Recycling overestimation

D. CONCLUSIONS

The effect of the Generation Region (GR) error plays a much stronger role on the calculated mobility values than does Photon Recycling (PR) because of the simultaneous effect PR has on diffusion length and lifetime. The PR effect is seen to grow as a function of doping.

The assumption of a 0.4μm error for GR is an estimate that needs more refinement, through the development of an analytical assessment of generation region definition and its inclusion in the numerical integration algorithm of

Appendix A. Transport Imaging provides an appropriate mechanism for this analysis and should be pursued.

The mobility values from the final corrected column are plotted against Dr. Bennett's predicted results with appropriate error bars in Figure 29.

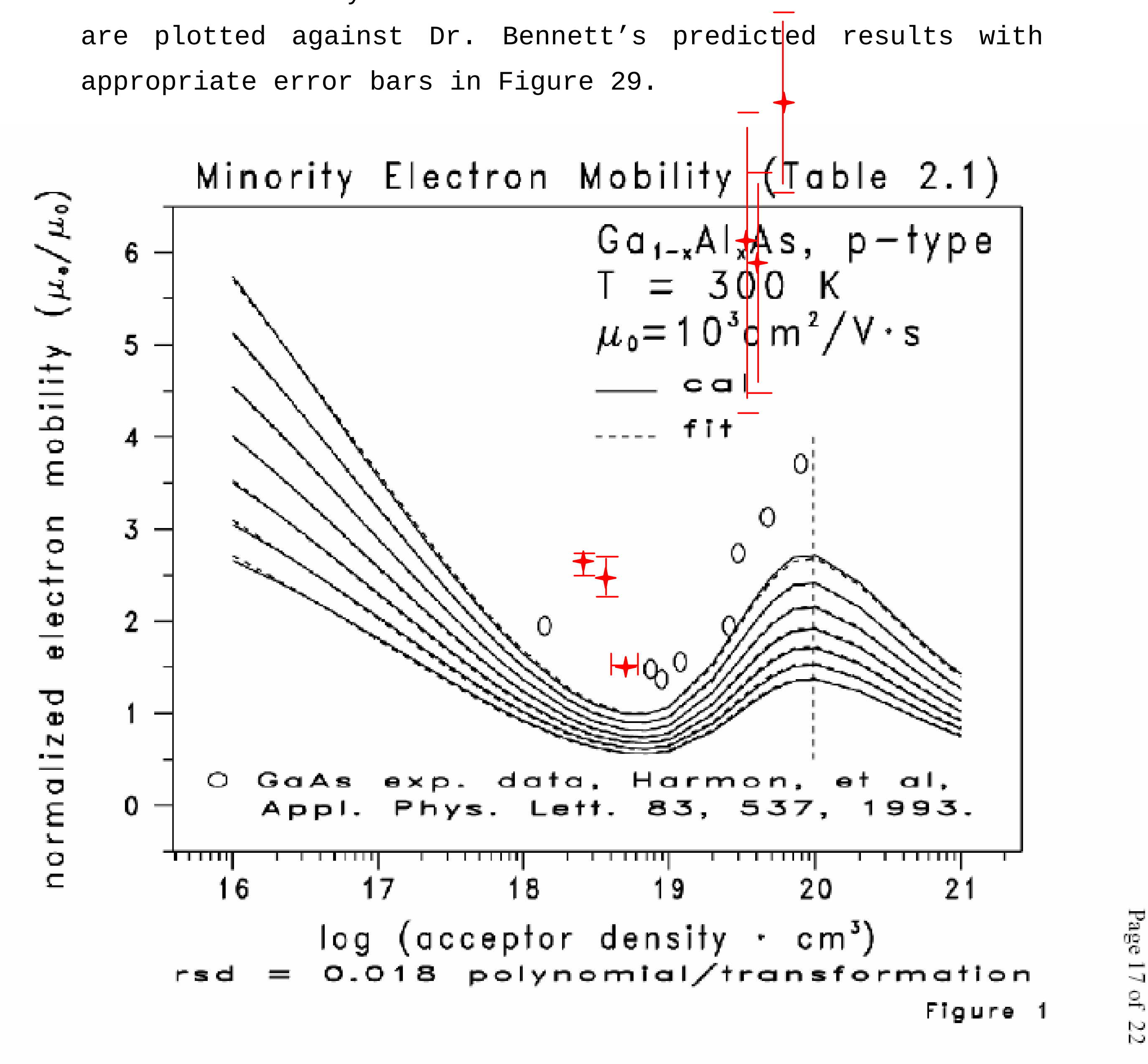

Figure 29. Final corrected Transport Imaging mobility values reported (After Bennett [9])

The local minimum is clearly demonstrated though absolute magnitude agreement is not. A new round of experiments is planned to test the magnitude relationships of the $\mu\tau$ product through the measurement of L_{drift} by studying the distributions as a result of an applied DC bias. In this manner a full distribution fit should escape the limitations resulting from generation region error, though the optical resolution limitation (0.4 μm) may still be operative in the samples of heaviest concentrations.

From the results demonstrated it can be assumed that of the limitations and constraints inherent in Transport Imaging the assumption of a generation region distribution has the largest impact for measurement of low diffusion length materials. It appears that experimental results can be assumed valid so long as the diffusion length measured is on the order of the generation region radius (as in Samples A9-C2), that the signal to noise ratio is favorable (as in all data samples shown herein), and that the diffusion lengths measured are greater than the optical resolution of the system (0.4μm in these data samples).

Several methods may be useful to overcome these constraints and are being studied in our laboratory. They include time resolved techniques reminiscent of the Haynes Shockley experiment, but maintaining the spatial information of the light emission to great resolution, AC drift techniques attempting to generate resonance responses between transport properties and the applied electric force, and observation of the effects of magnetic fields on the flow of the charge carriers at the sub micrometer scale.

APPENDIX A. TRANSPORT IMAGING GRAPHIC USER INTERFACE CODE

C:\Documents and Settings\FMBradley\My Documen...\newfirsttry.m Page 1
November 16, 2005 2:18:47 PM

```
function varargout = newfirsttry(varargin)

%-----------Log of program changes------------
%29 August - changed mkdir location for gui directory creation to create
%within diffusive data analysis\analyzed data.
%Will change parameter matching to Ld versus Mobility
%19 September - updated version on laptop with amended version from desktop
%12 October - Cleaned up comments and reorganized order of functions
%16 October - Reset all flag values in each main analysis functions (aflag,gflag, fitflag) all tested for empty variable status and set to '0' if so.

% NEWFIRSTTRY Application M-file for newfirsttry.fig
%   NEWFIRSTTRY, by itself, creates a new NEWFIRSTTRY or raises the existing
%   singleton*.
%
%   H = NEWFIRSTTRY returns the handle to a new NEWFIRSTTRY or the handle to
%   the existing singleton*.
%
%   NEWFIRSTTRY('CALLBACK',hObject,eventData,handles,...) calls the local
%   function named CALLBACK in NEWFIRSTTRY.M with the given input arguments.
%
%   NEWFIRSTTRY('Property','Value',...) creates a new NEWFIRSTTRY or raises the
%   existing singleton*.  Starting from the left, property value pairs are
%   applied to the GUI before newfirsttry_OpeningFunction gets called.  An
%   unrecognized property name or invalid value makes property application
%   stop.  All inputs are passed to newfirsttry_OpeningFcn via varargin.
%
%   *See GUI Options - GUI allows only one instance to run (singleton).
%
% See also: GUIDE, GUIDATA, GUIHANDLES

% Edit the above text to modify the response to help newfirsttry

% Last Modified by GUIDE v2.5 30-Mar-2005 12:09:12

% Begin initialization code - DO NOT EDIT

gui_Singleton = 1;
gui_State = struct('gui_Name',          mfilename, ...
                   'gui_Singleton',     gui_Singleton, ...
                   'gui_OpeningFcn',    @newfirsttry_OpeningFcn, ...
                   'gui_OutputFcn',     @newfirsttry_OutputFcn, ...
                   'gui_LayoutFcn',     [], ...
                   'gui_Callback',      []);
if nargin & isstr(varargin{1})
    gui_State.gui_Callback = str2func(varargin{1});
end

if nargout
```

```
    varargout{1:nargout} = gui_mainfcn(gui_State, varargin{:});
else
    gui_mainfcn(gui_State, varargin{:});
end
% End initialization code - DO NOT EDIT
%Initialize global variables
global aflag gflag foldername firsttime fitflag;
%aflag=0;
%gflag=0;
%fitflag=0;
%firsttime=0;
filetoload=[];

%________________________________________________________________________________________________________________________________________________

% --- Executes just before newfirsttry is made visible.
function newfirsttry_OpeningFcn(hObject, eventdata, handles, varargin)
% This function has no output args, see OutputFcn.
% hObject    handle to figure
% eventdata  reserved - to be defined in a future version of MATLAB
% handles    structure with handles and user data (see GUIDATA)
% varargin   command line arguments to newfirsttry (see VARARGIN)

% Choose default command line output for newfirsttry
handles.output = hObject;

% Update handles structure
guidata(hObject, handles);

if nargin == 3,
    initial_dir = pwd;
elseif nargin > 4
    if strcmpi(varargin{1},'dir')
        if exist(varargin{2},'dir')
            initial_dir = varargin{2};
        else
            errordlg('Input argument must be a valid directory','Input Argument Error!')
            return
        end
    else
        errordlg('Unrecognized input argument','Input Argument Error!');
        return;
    end
end
% Populate the listbox
load_listbox(initial_dir,handles)
% Return figure handle as first output argument

```

```
% UIWAIT makes newfirsttry wait for user response (see UIRESUME)
% uiwait(handles.newfirsttry);

%_________________________________________________________________________________________
_____________________________________________________________________
% --- Outputs from this function are returned to the command line.
function varargout = newfirsttry_OutputFcn(hObject, eventdata, handles)
% varargout  cell array for returning output args (see VARARGOUT);
% hObject    handle to figure
% eventdata  reserved - to be defined in a future version of MATLAB
% handles    structure with handles and user data (see GUIDATA)

% Get default command line output from handles structure
varargout{1} = handles.output;

% ________________________________________________________________________________________
____________________________________________________________________
% Callback for list box - open .fig with guide, otherwise use open
% ------------------------------------------------------------------
function varargout = listbox1_Callback(h, eventdata, handles)
% hObject    handle to listbox1 (see GCBO)
% eventdata  reserved - to be defined in a future version of MATLAB
% handles    structure with handles and user data (see GUIDATA)

% Hints: contents = get(hObject,'String') returns listbox1 contents as cell array
%        contents{get(hObject,'Value')} returns selected item from listbox1

get(handles.newfirsttry,'SelectionType');
global filetoload tiftoload ;

if strcmp(get(handles.newfirsttry,'SelectionType'),'open')
    index_selected = get(handles.listbox1,'Value');
    file_list = get(handles.listbox1,'String');
    filename = file_list{index_selected};
    if  handles.is_dir(handles.sorted_index(index_selected))
        cd (filename)
        load_listbox(pwd,handles)
    else
       [path,name,ext,ver] = fileparts(filename);
       switch ext
       case '.fig'
           guide (filename)
       case '.tif'
           tiftoload=filename;
       case '.csv'
           filetoload=filename;
       otherwise
        try
            filetoload=filename;
```

```
            catch
                errordlg(lasterr,'File Type Error','modal')
            end
        end
    end
end
% ______________________________________________________________________________________________________________
% Read the current directory and sort the names
% ------------------------------------------------------------
function load_listbox(dir_path,handles)
cd (dir_path)
dir_struct = dir(dir_path);
[sorted_names,sorted_index] = sortrows({dir_struct.name}');
handles.file_names = sorted_names;
handles.is_dir = [dir_struct.isdir];
handles.sorted_index = [sorted_index];
guidata(handles.newfirsttry,handles)
set(handles.listbox1,'String',handles.file_names,...
    'Value',1)
set(handles.text1,'String',pwd)

%____________________________________________________________________________________________________________________
% --- Executes during object creation, after setting all properties.
function listbox1_CreateFcn(hObject, eventdata, handles)
% hObject    handle to listbox1 (see GCBO)
% eventdata  reserved - to be defined in a future version of MATLAB
% handles    empty - handles not created until after all CreateFcns called

% Hint: listbox controls usually have a white background, change
%       'usewhitebg' to 0 to use default.  See ISPC and COMPUTER.
usewhitebg = 1;
if usewhitebg
    set(hObject,'BackgroundColor','white');
else
    set(hObject,'BackgroundColor',get(0,'defaultUicontrolBackgroundColor'));
end

%____________________________________________________________________________________________________________________
% --- Executes during object creation, after setting all properties.
function edit2_CreateFcn(hObject, eventdata, handles)
% hObject    handle to edit2 (see GCBO)
% eventdata  reserved - to be defined in a future version of MATLAB
% handles    empty - handles not created until after all CreateFcns called

% Hint: edit controls usually have a white background on Windows.
%       See ISPC and COMPUTER.
```

```
if ispc
    set(hObject,'BackgroundColor','white');
else
    set(hObject,'BackgroundColor',get(0,'defaultUicontrolBackgroundColor'));
end

%____________________________________________________________________________________________________________________________________

% --- Executes on mouse press over axes background.
function newname_ButtonDownFcn(hObject, eventdata, handles)
% hObject    handle to newname (see GCBO)
% eventdata  reserved - to be defined in a future version of MATLAB
% handles    structure with handles and user data (see GUIDATA)

%____________________________________________________________________________________________________________________________________
% --- Executes on button press in pushbutton1. (Vector Data Manipulator = vdatamanipulator)
function pushbutton1_Callback(hObject, eventdata, handles)
% hObject    handle to pushbutton1 (see GCBO)
% eventdata  reserved - to be defined in a future version of MATLAB
% handles    structure with handles and user data (see GUIDATA)
global filetoload aflag gflag foldername fitflag;
if (aflag==[]) aflag=0;
end
if (gflag==[]) gflag=0;
end
if (fitflag==[]) fitflag=0;
end
                    %Determine if this is a current session or a return to a previous session of data creation
button = questdlg('Are you in an active session of data analysis?','Session Type Selection');
switch button
    case 'Yes'
        nott='not';
        [Valmanac,xnplot,ynplot,xinterp,yinterp,sample_name,BeamEnergy,probe_current]=vdatamanipulator(filetoload, aflag, gflag, foldername);
        almanac_save(Valmanac,foldername,xnplot,ynplot,xinterp,yinterp,gflag,nott,filetoload);
        if fitflag
            datatofit=[xinterp;yinterp]';
            fbsLd(datatofit,foldername,sample_name,BeamEnergy,probe_current);
        end
case 'No'
        prompt = {'Enter the folder name for data plot storage','Enter name of superposition plot to amend'};
        dlg_title = 'Amended Session Input';
        num_lines= 1;
```

```
        def     = {'',''};
        answer  = inputdlg(prompt,dlg_title,num_lines,def);
        answerstr=char(answer);
        of=answer(1);
        oldfolder=char(of)
        superplotname=char(answerstr(2,:));
        [Valmanac,xnplot,ynplot,xinterp,yinterp,sample_name,BeamEnergy,probe_current]=vdatamanipulator(filetoload, aflag1, gflag1, oldfolder);
        almanac_save(Valmanac,oldfolder,xnplot,ynplot,xinterp,yinterp,gflag,superplotname,filetoload);
        if fitflag
            datatofit=[xinterp;yinterp]';
            fbsLd(datatofit,foldername,sample_name,BeamEnergy,probe_current);
        end
otherwise
        disp('To find the superplot and folder to amend, look in SEM\. Folder data sets are named by a 1xLetter designator denoting sample, followed by the beam energy.  The superplot is in this folder.')
end

%____________________________________________________________________________________________________________________________________________
% --- Executes on button press in pushbutton2 (ImageDataManipulator)
function pushbutton2_Callback(hObject, eventdata, handles)
% hObject    handle to pushbutton2 (see GCBO)
% eventdata  reserved - to be defined in a future version of MATLAB
% handles    structure with handles and user data (see GUIDATA)
global tiftoload foldername aflag gflag fitflag;
if (aflag==[]) aflag=0;
end
if (gflag==[]) gflag=0;
end
if (fitflag==[]) fitflag=0;
end
                                    %Determine if this is a current session or a return to a previous session of data creation
button = questdlg('Are you in an active session of data analysis?','Session Type Selection','Cancel');
switch button
    case 'Yes'
        nott='not';
        [almanacR, almanacC,xnplot,ynplot,xinterp,yinterp,sample_name,BeamEnergy,probe_current]=imagedatamanipulator(tiftoload, aflag, gflag, fitflag, foldername);
        almanac_save(almanacR,foldername,xnplot,ynplot,xinterp,yinterp,gflag,nott,tiftoload);
        flagc=0;                    %Sets the superimposition flag to '0' so column data will not be printed on superposition plot
        almanac_save(almanacC,foldername,xnplot,ynplot,xinterp,yinterp,flagc,nott,tiftoload);
```

```
        if fitflag
            datatofit=[xinterp;yinterp]';
            fbsLd(datatofit,foldername,sample_name,BeamEnergy,probe_current);
        end
    case 'No'
        prompt = {'Enter the folder name for data plot storage','Enter name of superposition plot to amend'};
        dlg_title = 'Amended Session Input';
        num_lines= 1;
        def     = {'',''};
        answer  = inputdlg(prompt,dlg_title,num_lines,def);
        answerstr=char(answer);
        oldfolder=(answerstr(1,:));
        superplotname=(answerstr(2,:));
        nott='not';          %Ensures that column data will not be
        [almanacR, almanacC,xnplot,ynplot,xinterp,yinterp,sample_name,BeamEnergy,probe_current]=imagedatamanipulator(tiftoload, aflag, gflag,fitflag, oldfolder);
        almanac_save(almanacR,foldername,xnplot,ynplot,xinterp,yinterp,gflag,superplotname,tiftoload);
        flagc=0;             %Sets the superimposition flag to '0' so column data will not be printed on superposition plot
        almanac_save(almanacC,foldername,xnplot,ynplot,xinterp,yinterp,flagc,nott,tiftoload);
        if fitflag
            datatofit=[xinterp;yinterp]';
            fbsLd(datatofit,foldername,sample_name,BeamEnergy,probe_current);
        end
    otherwise
   disp('To find the superplot and folder to amend, look in SEM\. Folder data sets are named by a 1xLetter designator denoting sample, followed by the beam energy.  The superplot is in this folder.')

end

%__________________________________________________________________________________________________________

% --- Executes on upcheck of checkbox1 = This is for 'Keep Almanac for mulitple files'.
function checkbox1_Callback(hObject, eventdata, handles)
% hObject    handle to checkbox1 (see GCBO)
% eventdata  reserved - to be defined in a future version of MATLAB
% handles    structure with handles and user data (see GUIDATA)
% Hint: get(hObject,'Value') returns toggle state of checkbox1
global aflag;
aflag = 1;

%__________________________________________________________________________________________________________

% --- Executes on upcheck of checkbox2 for superimposition box.
```

```
        [legend_h,object_h,plot_h,text_strings] = legend(gca);
        [n,m]=size(text_strings);
        counter=m/2;
        legendname=text_strings;
        if ishold
            yes=1;
        else hold on;
        end
        firsttime=0;
end
fid = fopen(['C:\Documents and Settings\FMBradley\My Documents\Physics\Data Analysis\',folder,'\Almanac.csv'],'a');
fprintf(fid,'%14.12f  %d %d %6.3f %d %6.3f\n',Dalmanac);
fclose(fid);
if firsttime==1                         %print superimposed graphs of row vector data
    legendname={};
    legendname=char(legendname);
    legendname=cellstr(legendname);
    counter=1;
    hold on;
    grid on;
    firsttime=0;
end
if flag == 1
    switch counter
          case {1}
            plot(xnplot,ynplot,'og');
            plot(xinterp,yinterp,'.g');
          case {2}
            plot(xnplot,ynplot,'ob');
            plot(xinterp,yinterp,'.b');
          case {3}
            plot(xnplot,ynplot,'oc');
            plot(xinterp,yinterp,'.c');
        case {4}
            plot(xnplot,ynplot,'ok');
            plot(xinterp,yinterp,'.k');
        case {5}
           plot(xnplot,ynplot,'om');
           plot(xinterp,yinterp,'.m');
        case {6}
            plot(xnplot,ynplot,'oy');
            plot(xinterp,yinterp,'.y');
        case {7}
            plot(xnplot,ynplot,'or');
            plot(xinterp,yinterp,'.r');
        case {8}
            plot(xnplot,ynplot,'sg');
            plot(xinterp,yinterp,'*g');
```

APPENDIX B. IMAGE DATA EXTRACTION ROUTINE (IMAGEDATAMANIPULATOR.M)

C:\Documents and Settings\FMBradley\M...\imagedatamanipulator.m   Page 1
November 16, 2005   5:44:29 PM

```

function [almanacR,almanacC,xnplot,ynplot,xinterp,yinterp,sample_name,BeamEnergy,probe_current]=imagedatamanipulator(tiftoload,aflag,gflag,fitflag,folder);

persistent fileserial;                                  %Allows var fileserial to hold value for an entire session of multiple calls to this fn
                                                        %if loop tests if variables are being saved to file,
                                                        %and increments fileserial
                                                        %to help differeniate
                                                        %figures
fileserial=fileserial+1;
%resets all figures and variables
%if ishold
 %   clf;
  %  hold off;
  %end

%read in image file
I0 = imread (tiftoload);
I0 = double(I0);
I0(:,1)=0;

%Initialize variables
Test=0;
m=0;
% Test for location of the spike of interest
[Y,I]=max(I0);      %Two vectors: Y=max value of each column, I=Row# of each columns Max)
[K,L]=size(I);      %K=row size, L=column size
MinVariance=300;
for m=1:(L-26)     %start test sequence at 1 go to length of indice matrix
 a=25;                 %test for remaining testable length less than 25 only take whats left
 for n=1:a          %Begin creation of test vector.  Populate with 25 elements of I (row # of max from each column)
        Test(n)=I((m+n));
 end
     Variance=std(Test); %Calculate variance of max values' row#s to select desired data sample.
 if Variance < MinVariance   %Update minimum variance
     MinVariance=Variance;
     seqstart=m;                %save indice start point in vector I of desired data sample (row #s of desired data sample)
     seqstop=m+a;
     seqlength=a;               %define sequence length to allow for seqlength to be used as indice addition term for creation of new vector.

 end
```

```
end
%Test Row data for least variance of column numbers for selected column data sample
I0T=I0';
[Y2,I3]=max(I0T);      %Two vectors: Y2=max value of each Row, I3=Col# of each row's Max)
[KR,LR]=size(I3);

MinVarianceR=500;
a=25;
for m3=2:(LR-a-1)           %Loop through all row numbers
    for n=1:a         %Begin creation of test vector.  Populate with 25 elements of I2 (Column # of max from each row)
       TestR(n)=I3((m3+n));
    end
VarianceR=std(TestR);            %Calculate variance of maximum values' column #s to select desired data sample.
 if VarianceR < MinVarianceR    %Update minimum variance
     MinVarianceR=VarianceR;
     seqstartR=m3;              %save indice start point in vector I2 of desired data sample (Column #s of desired data sample)
     seqstopR=m3+a;
     seqlengthR=a;              %define sequence length to allow for seqlength to be used as indice addition term for creation of new vector
 end
end

%Compare MaxValue vectors and choose column and row with largest same maximum
PeakPixelValue=0;
for stepR=1:25;
    for stepC=1:25;
       if Y(stepC+seqstart)==Y2(stepR+seqstartR)
        Peak=Y(stepC+seqstart);
        if Peak>PeakPixelValue
            PeakPixelValue=Peak;
            MaxPixelColNum=seqstart+stepC;
            MaxPixelRowNum=seqstartR+stepR;
        end
       end
    end
end

%extract row and column data
RowData=I0(MaxPixelRowNum,:);
ColData=I0(:,MaxPixelColNum);

%Create Noise vector from data outside of spike
%Calculate variance of noise and through out sample data vectors
for z=1:50
   NoiseData(z)=RowData(z);
```

```
end

RawVarOfNoise=std(NoiseData);
RawMeanOfNoise=mean(NoiseData);
for z1=1:50
    if NoiseData(z1) >= RawMeanOfNoise+RawVarOfNoise
        NoiseData(z1)=RawMeanOfNoise;
    end
end
MeanOfNoise=mean(NoiseData);        %Calculate average of noise within variance
VarOfNoise=std(NoiseData);
                                    %Normalize row vector of sample data
NormRowData=(RowData-MeanOfNoise)/(PeakPixelValue-MeanOfNoise);

                                    %Normalize ColData vector
for z=1:50
   NoiseDataCol(z)=ColData(z);
end

RawVarOfNoiseCol=std(NoiseDataCol);
RawMeanOfNoiseCol=mean(NoiseDataCol);
for z1=1:50
    if NoiseDataCol(z1) >= RawMeanOfNoiseCol+(2*RawVarOfNoiseCol)
        NoiseDataCol(z1)=RawMeanOfNoiseCol;
    end
end

%Calculate average of noise within variance
MeanOfNoiseCol=mean(NoiseDataCol);
VarOfNoiseCol=std(NoiseDataCol);
NormColData=(ColData-MeanOfNoiseCol)/(PeakPixelValue-MeanOfNoiseCol);

%add spline interpolation
    xr= (MaxPixelColNum-49):(MaxPixelColNum+50);
    xc= (MaxPixelRowNum-49):(MaxPixelRowNum+50);
for x1=1:100
    yr(x1) = NormRowData(MaxPixelColNum-50+x1);
    yc(x1)=NormColData(MaxPixelRowNum-50+x1);
end
       csc = spline(xc,[0 yc 0]);
       csr=spline(xr,[0 yr 0]);
       xxr=linspace((MaxPixelColNum-50),(MaxPixelColNum+50),1000);
       xxc = linspace((MaxPixelRowNum-50),(MaxPixelRowNum+50),1000);


%Extract Halfmaxfullwidth from the normalized Row data
maxdif=1;maxdify=1;
for xxx=1:500
```

```
    dif=abs(0.2-ppval(csr,xxr(xxx)));
    if dif<maxdif
        maxdif=dif;
        lhshalfmax=xxr(xxx);
    end
end
for xxy=500:1000
    dify=abs(0.2-ppval(csr,xxr(xxy)));
    if dify<maxdify
        maxdify=dify;
        rhshalfmax=xxr(xxy);
    end
end
hold;
Rhalfmaxfullwidth=rhshalfmax-lhshalfmax

%Extract the halfmaxfullwidth from the normalized column data
maxdif=.2;maxdify=.2;
for xxx=1:500
    dif=abs(0.2-ppval(csc,xxc(xxx)));
    if dif<maxdif
        maxdif=dif;
        lhshalfmax=xxc(xxx);
    end
end
for xxy=500:1000
    dify=abs(0.2-ppval(csc,xxc(xxy)));
    if dify<maxdify
        maxdify=dify;
        rhshalfmax=xxc(xxy);
    end
end
hold;
Chalfmaxfullwidth=rhshalfmax-lhshalfmax;

%Assign output variables to almanac vector
prompt = {'Unique sample name','Enter probe current in "3e-8" notation:','Enter Beam
Voltage in format "30" kV:','Enter Exposure Time in "10.005" (sec) format:'};
dlg_title = 'Almanac File Definition Input';
num_lines= 1;
def     = {'S72','6e-10','25','1.0'};
answer  = inputdlg(prompt,dlg_title,num_lines,def);
answerstr=char(answer);
sample_name=(answerstr(1,:));
probe_current=(answerstr(2,:));
BeamEnergystring=(answerstr(3,:));
BeamEnergy=str2double(answerstr(3,:));
ExpTime=str2double(answerstr(4,:));
almanacR=[sample_name str2double(probe_current) 0 BeamEnergy Rhalfmaxfullwidth PeakPi
```

```
xelValue ExpTime];
almanacC=[sample_name str2double(probe_current) 1 BeamEnergy Chalfmaxfullwidth PeakPi
xelValue ExpTime];



% Page 1 graphs. Overview of image with selected max values in colmax/row
% and rowmax/col
figure(1)
title(['Overview page for: ',folder,'_',tiftoload]);
subplot(3,1,1), imagesc(abs(I0));                          %Shows reproduction of tiff f
ile from MicroCCD
hold;
plot(MaxPixelColNum,MaxPixelRowNum,'xk');
title(['MATLAB reproduction of TIFF (',tiftoload,')']);
hold off;

% Plots maximum per Row vs Column number where that maximum falls in the row.
subplot(3,1,2), plot(max(I0));
hold;
title(['Max Pixel value/Row vs Column Number of MaxPixVal (',tiftoload,')']);
plot(MaxPixelColNum,(MeanOfNoise-VarOfNoise),'*y');
axis([0,L,(MeanOfNoise-VarOfNoise),(max(Y)+10)]);
grid on;
hold;

% Graph Columns' max pixel value vs row Number of MaxpixVal
subplot(3,1,3), plot(max(I0T));
hold;
title(['Max Pixel value/Column vs Row Number of MaxPixVal (',tiftoload,')']);
plot(MaxPixelRowNum,(MeanOfNoiseCol-VarOfNoiseCol),'*y');
axis([0,LR,(MeanOfNoiseCol-VarOfNoiseCol),(max(Y2)+10)]);
grid on;
hold;

%Save figure 1 to file
D=now;
ddate=day(D);
[n,mmonth]=month(D);
dateserial=['_',num2str(ddate),mmonth,num2str(fileserial)];
filetosave=['C:\Documents and Settings\FMBradley\My Documents\Physics\Data Analysis\'
,folder,'\OV',sample_name,'_',num2str(BeamEnergy),'_',probe_current,dateserial,'.fig'
];
saveas(1,filetosave);

%Write NormRowData to file
Vdatafile=['C:\Documents and Settings\FMBradley\My Documents\Physics\Data Analysis\',
folder,'\VRdata_',sample_name,'_',num2str(BeamEnergy),'_',probe_current,dateserial,'.
csv'];
```

```
fid = fopen(Vdatafile,'w');
fprintf(fid,'%11.9f\n',NormRowData);
fclose(fid);

%Write NormColData to file
Vdatafile=['C:\Documents and Settings\FMBradley\My Documents\Physics\Data Analysis\',
folder,'\VCdata_',sample_name,'_',num2str(BeamEnergy),'_',probe_current,dateserial,'.
csv'];
fid = fopen(Vdatafile,'w');
fprintf(fid,'%11.9f\n',NormColData);
fclose(fid);

%Plot Raw row and column data sets
figure(2);
title(['Peak plots for: ',folder,'_',tiftoload]);
%Raw Row and Column data
subplot(2,2,1), plot(RowData,'o');
title(['Raw Data for Peak Pixel Row (',tiftoload,')']);
axis([(MaxPixelColNum-50),(MaxPixelColNum+50),0,(PeakPixelValue+10)]);
grid on;
subplot(2,2,2), plot(ColData,'o');
title(['Col Data for Peak Pixel Column (',tiftoload,')']);
axis([(MaxPixelRowNum-50),(MaxPixelRowNum+50),0,(PeakPixelValue+20)]);
grid on;

%Print Normalized Row Data
R=0;xRlimit=0;xRstep=0;
[R,xRlimit]=size(NormRowData);
for xRstep=1:xRlimit;
    XRnorm(xRstep)=xRstep-MaxPixelColNum;
end
subplot(2,2,3), plot(XRnorm,NormRowData,'o');
hold;
plot((xxr-MaxPixelColNum),ppval(csr,xxr),'.');
title(['Normalized Row Data for Peak Pixel Row (',tiftoload,')']);
axis([(-50),(50),-.2,1.1]);
grid on;
text(10,0.5,['FWHM=',num2str(Rhalfmaxfullwidth)]);




%Print Column Data
[xlimit,C]=size(NormColData);
for xstep=1:xlimit;
    XCnorm(xstep)=xstep-MaxPixelRowNum;
end
subplot(2,2,4), plot(XCnorm,NormColData,'o');
hold;
```

```
plot((xxc-MaxPixelRowNum),ppval(csc,xxc),'.');
title(['Normalized Col Data for Peak Pixel Column (',tiftoload,')']);
axis([(-50),(50),-.2,1.1]);
grid on;
text(10,0.5,['FWHM=',num2str(Chalfmaxfullwidth)]);

%Save figure 2 to file
filetosave2=['C:\Documents and Settings\FMBradley\My Documents\Physics\Data Analysis\',folder,'\RC_',sample_name,'_',num2str(BeamEnergy),'_',probe_current, dateserial, '.fig'];
saveas(2, filetosave2);

%Test for desire for superimposed graph page and set export variables for
%consolidation in newfirsttry
if (or(gflag,fitflag))
    xnplot=XRnorm;
    ynplot=NormRowData;
    xinterp=xxr-MaxPixelColNum;
    yinterp=ppval(csr,xxr);
else
    xnplot=0;
    ynplot=0;
    xinterp=0;
    yinterp=0;
end
```

THIS PAGE INTENTIONALLY LEFT BLANK

APPENDIX C. LEAST SQUARES FIT ALGORITHM (FBSLD.M)


```
%------Created by FM Bradley to perform a least squares fit for data to the
%2-D model for diffusion of minority carriers in a luminscent
%semiconductor.

%Revision Log:  13 September - Time remaining window added by FMBradley

%Takes a 2-D vector data in (xstepX2) size, normalizes, cuts to 1% of max,
%performs a least squares fit to a 2-D model of carrier distro given a
%guassian distributed generation area.  Output is the fitted model vector,
%the difference between model and experimental data, plots of the parameter
%space, both curves, the selected of optimal Mu, and n=2sigma radius of
%generation area that fits the data.

function [FittedCurve,residue,Paramspace,Lopt,nopt]=fbsLd(datain,folder,sample_name,BeamEnergy,probe_current)

%CreateStruct.WindowStyle='replace';
 %    CreateStruct.Interpreter='tex';
  %   h=msgbox('Calculating.....','Progress Monitor',CreateStruct);
nmin=1e-4     %Significant radius of generation volume distribution(cm)  95% of current ring??
V=0;             %Applied bias (Volts)
%tau=4.32e-9;     %input variable.  Lifetime of carrier in question (s)
icd=1.0;         %inter-contact distance (mm) for calculation of electric field associated with V
E=V/icd*10;       %Electric field (V/cm)
step=0.04e-4;                          %step size in (cm)designed to fit the increment size of our experimental data w/interpolation
[R3,I3]=size(datain);                   %Id dimension of datain array
datain(:,1)=0.4e-4.*datain(:,1);         %Use this line if the data is coming from actual experimentally gathered and spline interpreted data from the MATLAB GUI.
                                         %Necessary because spline data is already in microns and we must convert all numbers here to cm

Lmin=SlopeL2(datain)-.3e-4;               %Conducts ln slope analysis method for the diffusion length assessment
Lstep=.1e-4;
stop=0;
while (stop<3)
    switch stop
        case 0
            Lstep=.2e-4;
            nstep=.2e-4;
            Lmax=Lmin+.4e-4;
            nmax=nmin+.4e-4;
        case 1
            Lstep=.1e-4;
            nstep=.1e-4;
            Lmax=Lmin+.2e-4;
```

```
            nmax=nmin+.2e-4;
        case 2
            Lstep=.1e-4;
            nstep=.1e-4;
            nmin=nmin-.5e-4;
            Lmin=Lmin-.5e-4;
            Lmax=Lmin+1e-4;
            nmax=nmin+1e-4;
    end

    a=0;            %step variable for indexing x
    b=0;            %step variable for indexing y
    MinSum=10000;
    istep=0;
    Paramspace=0;
    for L=Lmin:Lstep:Lmax
        t0=cputime;
        n=nmin;                                    %1-d spot dimension of a square generation area (cm)
        istep=istep+1;                             %parameter space indexing variable for mu
        jstep=0;                                   %param space index variable for n
        S=(E*L^2)/.025;                            %Field effect (cm)
        mtproduct=L^2/.025;                        %mu tau product in (cm^2/V)
        for n=nmin:nstep:nmax
            G=2/n;                                     %Gaussian 2sigma radius for 95% generation distro (unitless)
            jstep=jstep+1;
            xmin=datain(1,1);                      %convert datain from pixels to cm dependent upon resolution size of SEM/Optical scope .4microns/pixel
            xmax=max(datain(:,1));
            x=xmin;                                                          %(cm)
            ymin=0;                                                          %(cm)
            ymax=0;                                                          %(cm)
            y=ymin;
            b=0;
        for y1=ymin:step:ymax
          a=0;
          b=b+1;
            for x1=xmin:step:xmax
                Integrand=0;
                a=a+1;
                Integrand=dblquad(@Intgrnd,(x1-n),(x1+n),(y1-n),(y1+n),step,[],x1,y1,S,L,G);
                if (isnan(Integrand)) Integrand=OldIntegrand+.01*OldIntegrand;
```

```
                end
                OldIntegrand=Integrand;
                Int(a,b,1)=x1;
                Int(a,b,2)=y1;
                Int(a,b,3) = (G/(2*pi^2*L^2))*Integrand;
            end     %end x loop
        end     %end y loop
%Least square computation
            [M2,I2]=max(Int(:,1,3));
            NormInt=[Int(:,1,1) (Int(:,1,3)./M2)];
            %LogNormInt=log(NormInt(:,2));
            %LogDataIn=log(normdatain(:,2));
            LS=0;

        for loopc=1:R3;                         %1:(((dimofdata-1)/2)-105); %start loop at max +13 and count to end testing for least squares diff
            %LS(loopc)=(LogNormInt(I2+100+loopc)-LogDataIn(I3+100+loopc))^2
            %; Used to calculate log difference squares between two lines
            %of data
            if isnan(NormInt(loopc,2))
                NormInt(loopc,2)=1;
            end
            if isnan(datain(loopc,2))
                datain(loopc,2)=1;
            end
            if datain(loopc,2)<.7                                    %Eliminates the top 30% of the curve that does not fit our assumptions
            LS(loopc)=(NormInt(loopc,2)-datain(loopc,2))^2;
            end                                                      %ends non model fit data
        end                                                          %ends Least squares sum loop
        LoopSum=sum(LS);
        Paramspace(istep,jstep,1)=(istep-1)*Lstep+Lmin;
        Paramspace(istep,jstep,2)=(jstep-1)*nstep+nmin;
        Paramspace(istep,jstep,3)=LoopSum;
        if LoopSum<MinSum
            MinSum=LoopSum;
            residue=MinSum;
            ModelFit=NormInt;
            %Muopt=mu;
            nopt=n;
            Lopt=L;
            imin=istep;
            jmin=jstep;
        end
            figure(7);                     %Plot the search space each round of calculations complete
            nplot=n*1e4;
```

```
            Lplot=L*1e4;
            if (stop==1)plot(Lplot,nplot,'xr');
            else plot(Lplot,nplot,'xk');
            end
        if not(ishold) hold;
        end
    end                                                     %end of n for loop
   % CreateStruct.WindowStyle='replace';
   % CreateStruct.Interpreter='tex';
   % h=msgbox(['Total time remaining= ',num2str(((cputime-t0)/60)*(Lmax-L)/Lstep),' minutes. Step ',int2str(istep*jstep),' of ',num2str((((Lmax-Lmin)/Lstep)+1)*(((nmax-nmin)/nstep)+1)),' Total Steps'],'Progress Monitor',CreateStruct);
end                                                         %end of L for loop

%Decision tree for creating direction of propogation of parameter space
%build up.
switch imin
    case 1
        Lmin=Lmin-Lstep;
        if jmin==1
            nmin=nmin-nstep;
        elseif jmin==2
            nmin=nmin;
        else nmin=nmin+nstep;
        end
    case 2
        Lmin=Lmin;
        if jmin==1
            nmin=nmin-nstep;
        elseif jmin==3
            nmin=nmin+nstep;
        else
           stop=stop+1;
           plot((Lmin*1e4),(nmin*1e4),'xb');
       end
   case 3
       Lmin=Lmin+Lstep;
       if jmin==1
           nmin=nmin-nstep;
       elseif jmin==2
           nmin=nmin;
       else nmin=nmin+nstep;
       end
   otherwise
       break;
   end                                  %end for the switch loop
end                                  %end for the while loop
        title('Search Space');       %Label Figure 7
        xlabel('Ld (\mum)');
```

```
        ylabel('2\sigma (\mum)');
hold;                                %Hold off for figure 7
FittedCurve=ModelFit;
%Write Fitted Curve data to file
Vdatafile=['C:\Documents and Settings\FMBradley\My Documents\Physics\Data Analysis\',folder,'\ModelFit',sample_name,'Ld_',Lopt,'_',num2str(BeamEnergy),'kV_',probe_current,'.csv']
fid = fopen(Vdatafile,'w');
fprintf(fid,'%11.9f\n',ModelFit);
fclose(fid);
Residue=MinSum
nopt
Lopt


%plot the resulting fitted curves
figure(8);
plot(ModelFit(:,1),ModelFit(:,2),'.b',datain(:,1),datain(:,2),'-r');
hold on;
Xmax=xmax;
Xmin=xmin;
Ymin=0;
Ymax=1.0;
Axis([Xmin Xmax Ymin Ymax]);
title('Normalized Experimental vs. Model Fit');
xlabel('Radial distance from beam center (cm)');
ylabel('Normalized Intensity');
%'\mum:\mu=',num2str(Muopt),':\tau=',num2str(tau*1e9),
legendname1=['Model Fit:(n=',num2str(nopt*1e4),'\mum: Ld=',num2str(Lopt*1e4),'\mum) Residue=',num2str(residue)];
legendname2=['Data: ',sample_name,':PC=',num2str(probe_current),'Amps'];
legend(legendname1,legendname2);
hold off;


%Plot the parameter space of the resulting 1MicronX1Micron parameter range for both 2sigma and Ld
figure(9);
contour(Paramspace(:,:,2),Paramspace(:,:,1),Paramspace(:,:,3),100);
hold on;
plot(nopt,Lopt,'*y')
Xmax=nmax;
Xmin=nmin;
Ymin=Lmin;
Ymax=Lmax;
Axis([Xmin Xmax Ymin Ymax]);
title(['Parameter Space: ',sample_name,':',num2str(BeamEnergy),'kV:',num2str(probe_current),'A']);
ylabel('Ld step multiples [cm^2/Vs]');
```

```
xlabel('2\sigma steps of generation area [cm]');
colorbar('vert');
hold off;
```

APPENDIX D. VECTOR DATA EXTRACTION ROUTINE "VDATAMANIPULATOR.M"

C:\Documents and Settings\FMBradley\My Do...\vdatamanipulator.m Page 1
November 16, 2005 5:46:14 PM

```
function [almanacV,xnplot,ynplot,xinterp,yinterp,sample_name,BeamEnergy,probe_current]=vdatamanipulator(filetoload,aflag1,gflag1,foldername);

persistent fileserial;                          %Allows var fileserial to hold value for an entire session of multiple calls to this fn
                                                %if loop tests if variables are being saved to file,
                                                %and increments fileserial
                                                %to help differeniate
                                                %figures
fileserial=fileserial+1;

%resets all figures and variables
%if ishold
 %   clf;
  %  hold off;
  %end
%Row data input manipulation loop
%filename=input('Enter row data file name:','s');
rowdatainput=load(filetoload);
RowData=rowdatainput(:,2);

%Data preparation loop
[PeakPixelValue,MaxPixelColNum]=max(RowData);

%Create Noise vector from data outside of spike
%Calculate variance of noise and through out sample data vectors
for z=1:200
   NoiseData(z)=RowData(z);
end

RawVarOfNoise=std(NoiseData);
RawMeanOfNoise=mean(NoiseData);
for z1=1:200
    if NoiseData(z1) >= RawMeanOfNoise+RawVarOfNoise
        NoiseData(z1)=RawMeanOfNoise;
    end
end
MeanOfNoise=mean(NoiseData);         %Calculate average of noise within variance
VarOfNoise=std(NoiseData);
                                     %Normalize row vector of sample data
NormRowData=(RowData-MeanOfNoise)/(PeakPixelValue-MeanOfNoise);


%add spline interpolation
    xr= (MaxPixelColNum-49):(MaxPixelColNum+50);
for x1=1:100
    yr(x1) = NormRowData(MaxPixelColNum-50+x1);
end
```

```
        csr=spline(xr,[0 yr 0]);
        xxr=linspace((MaxPixelColNum-50),(MaxPixelColNum+50),1000);

%Extract Halfmaxfullwidth from the normalized Row data
maxdif=1;maxdify=1;
for xxx=1:500
    dif=abs(0.2-ppval(csr,xxr(xxx)));
    if dif<maxdif
        maxdif=dif;
        lhshalfmax=xxr(xxx);
    end
end
for xxy=500:1000
    dify=abs(0.2-ppval(csr,xxr(xxy)));
    if dify<maxdify
        maxdify=dify;
        rhshalfmax=xxr(xxy);
    end
end
Rhalfmaxfullwidth=rhshalfmax-lhshalfmax;

%Assign output variables to almanac vector
prompt = {'Unique sample name','Enter probe current in "3e-8" notation:','Enter Beam Voltage in format "30" kV:','Enter Exposure Time in "10.005" (sec) format:','Enter R or C for Row or Column Data'};
dlg_title = 'Almanac File Definition Input';
num_lines= 1;
def     = {'S72','6e-10','25','1.0','R'};
answer  = inputdlg(prompt,dlg_title,num_lines,def);
answerstr=char(answer);
sample_name=(answerstr(1,:));
probe_current=(answerstr(2,:));
BeamEnergystring=(answerstr(3,:));
BeamEnergy=str2double(answerstr(3,:));
ExpTime=str2double(answerstr(4,:));
switch answerstr(5)
    case 'R'
        vector_type='0';
    case 'C'
        vector_type='1';
    otherwise
        dialg('Your test did not work');
end
almanacV=[str2double(probe_current) vector_type BeamEnergy Rhalfmaxfullwidth PeakPixelValue ExpTime];

%Analysis output loop
%Plot Raw row and column data sets
figure(1);
```

```
%Plot overview graph of row
subplot(1,2,1), plot(RowData,'o');
title(['Raw Data for Peak Pixel Vector (',foldername,filetoload,')']);
axis([(MaxPixelColNum-50),(MaxPixelColNum+50),0,(PeakPixelValue+10)]);
grid on;

%Print Row Data
[xRlimit,R]=size(NormRowData);
for xRstep=1:xRlimit;
    XRnorm(xRstep)=xRstep-MaxPixelColNum;
end
subplot(1,2,2), plot(XRnorm,NormRowData,'o');
hold;
plot((xxr-MaxPixelColNum),ppval(csr,xxr),'.');
title(['Normalized Data for Peak Pixel Vector (',filetoload,')']);
axis([(-50),(50),-.2,1.1]);
grid on;
text(10,0.5,['FWHM=',num2str(Rhalfmaxfullwidth)]);
hold;

%Save figure 1 to file
D=now;
ddate=day(D);
[n,mmonth]=month(D);
dateserial=['_',num2str(ddate),mmonth,num2str(fileserial)];
filetosave=['C:\Documents and Settings\FMBradley\My Documents\Physics\Data Analysis\',foldername,'\',answerstr(4),num2str(BeamEnergy),'_',probe_current,dateserial,'.fig'];
saveas(1,filetosave);
figure(2);

%Set export variables for
%consolidation in newfirsttry
        xnplot=XRnorm;
        ynplot=NormRowData;
        xinterp=xxr-MaxPixelColNum;
        yinterp=ppval(csr,xxr);
```

THIS PAGE INTENTIONALLY LEFT BLANK

APPENDIX E. SLOPE ANALYSIS ALGORITHM (SLOPEL2.M)

C:\Documents and Settings\FMBradley\My Documents\P...\SlopeL2.m Page 1
November 16, 2005 5:45:34 PM

```
function [L]=SlopeL(datavector)
%
%
%--------------------------------Automated slope determination algorithym
%to gain initial indication of diffusion length of a material.
%  Original protocol determined by Dave Luber.  Automated by Mitch Bradley
%  3 October, 2005
j=1;
y=0;
i=1;
[V,I]=max(datavector(:,2));
EOV=size(datavector(:,1));
for i=1:I
y=datavector(i,2);
if(y<.1)                %These limits should be adjusted for noise level of the sample image (2OOM above lower limit)
    if (y>.01)                %This should be adjusted for lower limit of noise level for sample image
        yfit(j)=log(y);
        xfit(j)=datavector(i,1);
        j=j+1;
    end
    %i=i+1;
end
end
p=polyfit(xfit,yfit,1);                %conduct polylinomial fit for poly of degree 1 (linear) for data in xfit and yfit
L=1/p(1)
b=p(2)
fitdata=[xfit', yfit'];

%_____________________Loop for the right side of the distribution_____________________________________
j=1;
for i=I:EOV
yr=datavector(i,2);
if(yr<.1)                %These limits should be adjusted for noise level of the sample image (2OOM above lower limit)
    if (yr>.01)                %This should be adjusted for lower limit of noise level for sample image
        yfitr(j)=log(yr);
        xfitr(j)=datavector(i,1);
        j=j+1;
    end
    %i=i+1;
end
end
pr=polyfit(xfitr,yfitr,1);                %conduct polylinomial fit for poly of degree 1 (linear) for data in xfit and yfit
```

```
Lr=-1/pr(1)
br=pr(2)
fitdataR=[xfitr', yfitr'];

%-----Plot ln(Intensity) vs X pos for all data left of spot------
figure(4);
plot(datavector(:,1),log(datavector(:,2)));
%axis([(datavector(1,1)),(0),(log(min(datavector(:,2)))),(0)]);
title('LN(Intensity) of Left Side Distribution');
xlabel('Radial distance from beam center (cm)');
ylabel('LN(Normalized Intensity)');

%-----Calculate error reports and plot line slopes------
figure(5);
Lplus=L+(.4e-4)/(max(yfit)-yfit(1));            %The Plus factor should be .4e-4 for real data and .04e-4 for tfbs control data
Lminus=L-(.4e-4)/(max(yfit)-yfit(1));           %The minus factor should be .4e-4 for real data and .04e-4 for tfbs control data
plot(xfit,yfit,'ob');
hold;
plot(xfit,polyval(p,xfit),'-r');
yplus=(1/Lplus)*xfit+b;
yminus=(1/Lminus)*xfit+b;
plot(xfit,yplus,'-g');
plot(xfit,yminus,'-k');
%_________________________Right side___________________________
Lplusr=Lr+(.4e-4)/(max(yfitr)-min(yfitr));            %The Plus factor should be .4e-4 for real data and .04e-4 for tfbs control data
Lminusr=Lr-(.4e-4)/(max(yfitr)-min(yfitr));           %The minus factor should be .4e-4 for real data and .04e-4 for tfbs control data
plot(xfitr,yfitr,'ob');
plot(xfitr,polyval(pr,xfitr),'-r');
yplusr=(-1/Lplusr)*xfitr+br;
yminusr=(-1/Lminusr)*xfitr+br;
plot(xfitr,yplusr,'-g');
plot(xfitr,yminusr,'-k');

legendname1=['Data Points'];
legendname2=['L actual Ld=',num2str(L*1e4),'\mum'];
legendname3=['L Ld(+)=',num2str(Lplus*1e4),'\mum'];
legendname4=['L Ld(-)=',num2str(Lminus*1e4),'\mum'];
legendname5=['Data Points'];
legendname6=['R actual Ld=',num2str(Lr*1e4),'\mum'];
legendname7=['R Ld(+)=',num2str(Lplusr*1e4),'\mum'];
legendname8=['R Ld(-)=',num2str(Lminusr*1e4),'\mum'];


legend(legendname1,legendname2,legendname3,legendname4,legendname5,legendname6,legendname7,legendname8);
```

```
title('Slope Analysis Estimate of Ld');
xlabel('Radial distance from beam center (cm)');
ylabel('LN(Normalized Intensity)');
hold;
```

THIS PAGE INTENTIONALLY LEFT BLANK

APPENDIX F. NUMERICAL INTEGRATION SOLUTION FOR MINORITY CARRIER DISTRIBUTION (INTEGRAND.M)

C:\Documents and Settings\FMBradley\My Documents\P...\Intgrnd.m Page 1
November 16, 2005 5:45:03 PM

```
function I=Intgrnd(chi,ada,x1,y1,S,L,G)
I=exp(-(G^2).*((x1-chi).^2+(y1-ada).^2)+(S.*chi/(2*L.^2))).*besselk(0,(sqrt((S.^2+4*L.^2).*(chi.^2+ada.^2))/(2*L.^2)));
%I=exp(S.*chi/(2*L.^2)).*besselk(0,(sqrt(S.^2+4*L.^2).*(chi.^2+ada.^2).^(.5)/(2*L.^2)));

```

THIS PAGE INTENTIONALLY LEFT BLANK

APPENDIX G. PHOTON RECYCLING PERTURBATION

REFERENCE EQUATION SHEET

Calculated Properties — **Measured Properties** — **Referenced Properties**

$\tau_{radiative} = t := \dfrac{1}{2\cdot 10^{-10}\cdot Na}$ $\quad Na :=$ $\quad \alpha :=$ $\quad \theta 1 := 1.21 \quad R1 := .001$

$Lm :=$ $\quad \theta 2 := 1.21 \quad R2 := .001$

$t =$ $\quad \tau :=$ $\quad L\alpha = \dfrac{1}{\alpha} =$ $\quad w := 1\cdot\left(10^{-4}\right)$

$Dm = \dfrac{Lm^2}{\tau} \quad Dm =$

$$E(n,z) := \int_1^{\infty} \frac{e^{-z\cdot t}}{t^n}\,dt$$

$$T0 := \left[\left[(1-R1)\cdot\cos(\theta 1)\cdot\frac{-2E\left(3,\alpha\cdot\frac{w}{\cos(\theta 1)}\right)+E\left(3,2\alpha\cdot\frac{w}{\cos(\theta 1)}\right)+\frac{1}{2}}{2\alpha\cdot w\cdot t}\right]+\frac{1+\left(E(3,\alpha\cdot w)-\frac{1}{2}\right)\cdot\frac{1}{\alpha\cdot w}+\left(-2E(3,\alpha\cdot w)+E(3,2\alpha\cdot w)+\frac{1}{2}\right)\cdot\frac{R2+R1}{2\alpha\cdot w}}{t}+\frac{\left(\frac{\cos(\theta 1)^2}{\alpha\cdot w}\cdot\frac{1-R1}{2}\right)\cdot\left(-2E\left(3,\alpha\cdot\frac{w}{\cos(\theta 1)}\right)+E\left(3,2\cdot w\frac{\alpha}{\cos(\theta 1)}\right)+\frac{1}{2}\right)}{t}\right]$$

$T0 =$ $\quad \tau a := \left[\left(\dfrac{1}{\tau}\right)+(T0)\right]^{-1}$ $\quad \tau a =$

$$T2 := \left(\frac{1}{t\cdot w}\right)\cdot\left[\frac{(1-R2)\cdot\cos(\theta 2)^2\cdot\left[\frac{\cos(\theta 2)^2\cdot\left(-2E\left(5,\alpha\cdot\frac{w}{\cos(\theta 2)}\right)+E\left(5,2\alpha\cdot\frac{w}{\cos(\theta 2)}\right)+\frac{1}{4}\right)}{\alpha^3}+-E\left(3,\alpha\cdot\frac{w}{\cos(\theta 2)}\right)\cdot\frac{w^2}{\alpha}\right]}{2\alpha}+\frac{(1-R1)\cdot\cos(\theta 1)^2\cdot\left[\frac{\cos(\theta 1)^2\cdot\left(-2E\left(5,\alpha\cdot\frac{w}{\cos(\theta 1)}\right)+E\left(5,2\alpha\cdot\frac{w}{\cos(\theta 1)}\right)+\frac{1}{4}\right)}{\alpha^3}+-E\left(3,\alpha\cdot\frac{w}{\cos(\theta 1)}\right)\cdot\frac{w^2}{\alpha}\right]}{2\alpha}+\frac{(R2+R1)\cdot\left[-E(3,w\alpha)\cdot\left(\frac{w^2}{\alpha}\right)+\frac{1\cdot\left(-2E(5,\alpha\cdot w)+E(5,2\alpha\cdot w)+\frac{1}{4}\right)}{\alpha^3}\right]}{2}+\frac{3\left(E(5,w\alpha)-\frac{1}{4}\right)}{\alpha^3}+\left(\frac{E(3,\alpha\cdot w)\cdot w^2}{2\alpha}\right)+\frac{w\left(2E(4,\alpha\cdot w)+\frac{1}{3}\ldots\right)}{\alpha^2}\right.$$

$T2 =$ $\quad Da = Dm - T2$ $\quad La = \sqrt{Da\cdot\tau a}$ $\quad La =$

$Da =$ $\quad \mu := \dfrac{Da}{.025}$ $\quad \mu =$

SAMPLE D6

Calculated Properties — **Measured Properties** — **Referenced Properties**

$\tau_{radiative} = t := \dfrac{1}{2\cdot 10^{-10}\cdot Na}$ $\quad Na := 3.5\cdot 10^{19}$ $\quad \alpha := 3500$ $\quad \theta 1 := 1.21 \quad R1 := .001$

$Lm := 1.2\cdot 10^{-4}$ $\quad \theta 2 := 1.21 \quad R2 := .001$

$t = 1.429\times 10^{-10}$ $\quad \tau := 95\cdot 10^{-12}$ $\quad L\alpha = \dfrac{1}{\alpha} = 2.857\times 10^{-4}$ $\quad w := 1\cdot\left(10^{-4}\right)$

$Dm = \dfrac{Lm^2}{\tau} \quad Dm = 151.579$

$$E(n,z) := \int_1^{\infty} \frac{e^{-z\cdot t}}{t^n}\,dt$$

$$T0 := \left[\left[(1-R1)\cdot\cos(\theta 1)\cdot\frac{-2E\left(3,\alpha\cdot\frac{w}{\cos(\theta 1)}\right)+E\left(3,2\alpha\cdot\frac{w}{\cos(\theta 1)}\right)+\frac{1}{2}}{2\alpha\cdot w\cdot t}\right]+\frac{1+\left(E(3,\alpha\cdot w)-\frac{1}{2}\right)\cdot\frac{1}{\alpha\cdot w}+\left(-2E(3,\alpha\cdot w)+E(3,2\alpha\cdot w)+\frac{1}{2}\right)\cdot\frac{R2+R1}{2\alpha\cdot w}}{t}+\frac{\left(\frac{\cos(\theta 1)^2}{\alpha\cdot w}\cdot\frac{1-R1}{2}\right)\cdot\left(-2E\left(3,\alpha\cdot\frac{w}{\cos(\theta 1)}\right)+E\left(3,2\cdot w\frac{\alpha}{\cos(\theta 1)}\right)+\frac{1}{2}\right)}{t}\right]$$

$T0 = 4.029\times 10^{9}$ $\quad \tau a := \left[\left(\dfrac{1}{\tau}\right)+(T0)\right]^{-1}$ $\quad \tau a = 6.87\times 10^{-11}$

$$T2 := \left(\frac{1}{t\cdot w}\right)\cdot\left[\frac{(1-R2)\cdot\cos(\theta 2)^2\cdot\left[\frac{\cos(\theta 2)^2\cdot\left(-2E\left(5,\alpha\cdot\frac{w}{\cos(\theta 2)}\right)+E\left(5,2\alpha\cdot\frac{w}{\cos(\theta 2)}\right)+\frac{1}{4}\right)}{\alpha^3}+-E\left(3,\alpha\cdot\frac{w}{\cos(\theta 2)}\right)\cdot\frac{w^2}{\alpha}\right]}{2\alpha}+\frac{(1-R1)\cdot\cos(\theta 1)^2\cdot\left[\frac{\cos(\theta 1)^2\cdot\left(-2E\left(5,\alpha\cdot\frac{w}{\cos(\theta 1)}\right)+E\left(5,2\alpha\cdot\frac{w}{\cos(\theta 1)}\right)+\frac{1}{4}\right)}{\alpha^3}+-E\left(3,\alpha\cdot\frac{w}{\cos(\theta 1)}\right)\cdot\frac{w^2}{\alpha}\right]}{2\alpha}+\frac{(R2+R1)\cdot\left[-E(3,w\alpha)\cdot\left(\frac{w^2}{\alpha}\right)+\frac{1\cdot\left(-2E(5,\alpha\cdot w)+E(5,2\alpha\cdot w)+\frac{1}{4}\right)}{\alpha^3}\right]}{2}+\frac{3\left(E(5,w\alpha)-\frac{1}{4}\right)}{\alpha^3}+\left(\frac{E(3,\alpha\cdot w)\cdot w^2}{2\alpha}\right)+\frac{w\left(2E(4,\alpha\cdot w)+\frac{1}{3}\ldots\right)}{\alpha^2}\right.$$

$T2 = 1.282$ $\quad Da = Dm - T2$ $\quad La = \sqrt{Da\cdot\tau a}$ $\quad La = 1.016\times 10^{-4}$

$Da = 150.297$ $\quad \mu := \dfrac{Da}{.025}$ $\quad \mu = 6.012\times 10^{3}$

SAMPLE E3

Calculated Properties — **Measured Properties** — **Referenced Properties**

$\tau_{radiative} = t := \dfrac{1}{2\cdot 10^{-10}\cdot Na}$ $\quad Na := 4\cdot 10^{19}$ $\quad \alpha := 3400$ $\quad \theta 1 := 1.21 \quad R1 := .001$

$Lm := 1.4\cdot 10^{-4}$ $\quad \theta 2 := 1.21 \quad R2 := .001$

$t = 1.25\times 10^{-10}$ $\quad \tau := 140\cdot 10^{-12}$ $\quad L\alpha = \dfrac{1}{\alpha} = 2.941\times 10^{-4}$ $\quad w := 1\cdot\left(10^{-4}\right)$

$Dm = \dfrac{Lm^2}{\tau} \quad Dm = 140$

$$E(n,z) := \int_1^{\infty} \frac{e^{-z\cdot t}}{t^n}\,dt$$

$$T0 := \left[\left[(1-R1)\cdot\cos(\theta 1)\cdot\frac{-2E\left(3,\alpha\cdot\frac{w}{\cos(\theta 1)}\right)+E\left(3,2\alpha\cdot\frac{w}{\cos(\theta 1)}\right)+\frac{1}{2}}{2\alpha\cdot w\cdot t}\right]+\frac{1+\left(E(3,\alpha\cdot w)-\frac{1}{2}\right)\cdot\frac{1}{\alpha\cdot w}+\left(-2E(3,\alpha\cdot w)+E(3,2\alpha\cdot w)+\frac{1}{2}\right)\cdot\frac{R2+R1}{2\alpha\cdot w}}{t}+\frac{\left(\frac{\cos(\theta 1)^2}{\alpha\cdot w}\cdot\frac{1-R1}{2}\right)\cdot\left(-2E\left(3,\alpha\cdot\frac{w}{\cos(\theta 1)}\right)+E\left(3,2\cdot w\frac{\alpha}{\cos(\theta 1)}\right)+\frac{1}{2}\right)}{t}\right]$$

$T0 = 4.57\times 10^{9}$ $\quad \tau a := \left[\left(\dfrac{1}{\tau}\right)+(T0)\right]^{-1}$ $\quad \tau a = 8.538\times 10^{-11}$

$$T2 := \left(\frac{1}{t\cdot w}\right)\cdot\left[\frac{(1-R2)\cdot\cos(\theta 2)^2\cdot\left[\frac{\cos(\theta 2)^2\cdot\left(-2E\left(5,\alpha\cdot\frac{w}{\cos(\theta 2)}\right)+E\left(5,2\alpha\cdot\frac{w}{\cos(\theta 2)}\right)+\frac{1}{4}\right)}{\alpha^3}+-E\left(3,\alpha\cdot\frac{w}{\cos(\theta 2)}\right)\cdot\frac{w^2}{\alpha}\right]}{2\alpha}+\frac{(1-R1)\cdot\cos(\theta 1)^2\cdot\left[\frac{\cos(\theta 1)^2\cdot\left(-2E\left(5,\alpha\cdot\frac{w}{\cos(\theta 1)}\right)+E\left(5,2\alpha\cdot\frac{w}{\cos(\theta 1)}\right)+\frac{1}{4}\right)}{\alpha^3}+-E\left(3,\alpha\cdot\frac{w}{\cos(\theta 1)}\right)\cdot\frac{w^2}{\alpha}\right]}{2\alpha}+\frac{(R2+R1)\cdot\left[-E(3,w\alpha)\cdot\left(\frac{w^2}{\alpha}\right)+\frac{1\cdot\left(-2E(5,\alpha\cdot w)+E(5,2\alpha\cdot w)+\frac{1}{4}\right)}{\alpha^3}\right]}{2}+\frac{3\left(E(5,w\alpha)-\frac{1}{4}\right)}{\alpha^3}+\left(\frac{E(3,\alpha\cdot w)\cdot w^2}{2\alpha}\right)+\frac{w\left(2E(4,\alpha\cdot w)+\frac{1}{3}\ldots\right)}{\alpha^2}\right.$$

$T2 = 1.45$ $\quad Da = Dm - T2$ $\quad La = \sqrt{Da\cdot\tau a}$ $\quad La = 1.088\times 10^{-4}$

$Da = 138.55$ $\quad \mu := \dfrac{Da}{.025}$ $\quad \mu = 5.542\times 10^{3}$

SAMPLE F4

Calculated Properties | **Measured Properties** | **Referenced Properties**

$Na := 6\cdot 10^{19}$

$\tau_{radiative} = t := \frac{1}{2\cdot 10^{-10}\cdot Na}$

$t = 8.333\times 10^{-11}$

$Lm := 1.5\cdot 10^{-4}$

$\tau := 116\cdot 10^{-12}$

$\alpha := 3000$ $\quad \theta1 := 1.21 \quad R1 := .001$

$\theta2 := 1.21 \quad R2 := .001$

$L\alpha := \frac{1}{\alpha} = 3.333\times 10^{-4}$ $\quad w := 1\cdot\left(10^{-4}\right)$

$Dm := \frac{Lm^2}{\tau}$ $\quad Dm = 193.966$

$$E(n,z) := \int_1^{\infty} \frac{e^{-z\cdot t}}{t^n}\,dt$$

$$T0 := \left[\left[(1-R1)\cdot\cos(\theta1)\cdot\frac{-2\cdot E\left(3,\alpha\cdot\frac{w}{\cos(\theta1)}\right)+E\left(3,2\alpha\cdot\frac{w}{\cos(\theta1)}\right)+\frac{1}{2}}{2\cdot\alpha\cdot w\cdot t}\right]+\frac{1+\left(E(3,\alpha\cdot w)-\frac{1}{2}\right)\cdot\frac{1}{\alpha\cdot w}+\left(-2\cdot E(3,\alpha\cdot w)+E(3,2\cdot\alpha\cdot w)+\frac{1}{2}\right)\cdot\frac{R2+R1}{2\cdot\alpha\cdot w}}{t}+\frac{\left(\frac{\cos(\theta1)^2}{\alpha\cdot w}\cdot\frac{1-R1}{2}\right)\cdot\left(-2\cdot E\left(3,\alpha\cdot\frac{w}{\cos(\theta1)}\right)+E\left(3,2\cdot w\cdot\frac{\alpha}{\cos(\theta1)}\right)+\frac{1}{2}\right)}{t}\right]$$

$T0 = 6.626\times 10^{9}$ $\quad \tau a := \left[\left(\frac{1}{\tau}\right)+(T0)\right]^{-1}$ $\quad \tau a = 6.559\times 10^{-11}$

$$T2 := \left(\frac{1}{t\cdot w}\right)\cdot\left[\frac{(1-R2)\cdot\cos(\theta2)^2\cdot\left[\frac{\cos\left(\theta2^2\right)\cdot\left(-2\cdot E\left(5,\alpha\cdot\frac{w}{\cos(\theta2)}\right)+E\left(5,2\alpha\cdot\frac{w}{\cos(\theta2)}\right)+\frac{1}{4}\right)}{\alpha^3}+-E\left(3,\alpha\cdot\frac{w}{\cos(\theta2)}\right)\cdot\frac{w^2}{\alpha}\right]}{2\alpha}+\frac{(1-R1)\cdot\cos(\theta1)^2\cdot\left[\frac{\cos\left(\theta1^2\right)\cdot\left(-2\cdot E\left(5,\alpha\cdot\frac{w}{\cos(\theta1)}\right)+E\left(5,2\alpha\cdot\frac{w}{\cos(\theta1)}\right)+\frac{1}{4}\right)}{\alpha^3}+-E\left(3,\alpha\cdot\frac{w}{\cos(\theta1)}\right)\cdot\frac{w^2}{\alpha}\right]}{2\alpha}+\frac{(R2+R1)\cdot\left[-E(3,w\alpha)\cdot\left(\frac{w^2}{\alpha}\right)+\frac{1\cdot\left(-2E(5,\alpha\cdot w)+E(5,2\alpha\cdot w)+\frac{1}{4}\right)}{\alpha^3}\right]}{2}+\frac{3\cdot\left(E(5,w\alpha)-\frac{1}{4}\right)}{\alpha^3}+\left(\frac{E(3,\alpha\cdot w)\cdot w^2}{2\alpha}\right)+\frac{w\cdot\left(2E(4,\alpha\cdot w)+\cdots\right)}{\alpha^2}\right.$$

$T2 = 2.075$ $\quad Da := Dm - T2$ $\quad La := \sqrt{Da\cdot\tau a}$ $\quad La = 1.122\times 10^{-4}$

$Da = 191.89$ $\quad \mu := \frac{Da}{.025}$ $\quad \mu = 7.676\times 10^{3}$

SAMPLE G8

Calculated Properties | **Measured Properties** | **Referenced Properties**

$Na := 1\cdot 10^{20}$

$\tau_{radiative} = t := \frac{1}{2\cdot 10^{-10}\cdot Na}$

$t = 5\times 10^{-11}$

$Lm := 1.0\cdot 10^{-4}$

$\tau := 11\cdot 10^{-12}$

$\alpha := 2300$ $\quad \theta1 := 1.21 \quad R1 := .001$

$\theta2 := 1.21 \quad R2 := .001$

$L\alpha := \frac{1}{\alpha} = 4.348\times 10^{-4}$ $\quad w := 1\cdot\left(10^{-4}\right)$

$Dm := \frac{Lm^2}{\tau}$ $\quad Dm = 909.091$

$$E(n,z) := \int_1^{\infty} \frac{e^{-z\cdot t}}{t^n}\,dt$$

$$T0 := \left[\left[(1-R1)\cdot\cos(\theta1)\cdot\frac{-2\cdot E\left(3,\alpha\cdot\frac{w}{\cos(\theta1)}\right)+E\left(3,2\alpha\cdot\frac{w}{\cos(\theta1)}\right)+\frac{1}{2}}{2\cdot\alpha\cdot w\cdot t}\right]+\frac{1+\left(E(3,\alpha\cdot w)-\frac{1}{2}\right)\cdot\frac{1}{\alpha\cdot w}+\left(-2\cdot E(3,\alpha\cdot w)+E(3,2\cdot\alpha\cdot w)+\frac{1}{2}\right)\cdot\frac{R2+R1}{2\cdot\alpha\cdot w}}{t}+\frac{\left(\frac{\cos(\theta1)^2}{\alpha\cdot w}\cdot\frac{1-R1}{2}\right)\cdot\left(-2\cdot E\left(3,\alpha\cdot\frac{w}{\cos(\theta1)}\right)+E\left(3,2\cdot w\cdot\frac{\alpha}{\cos(\theta1)}\right)+\frac{1}{2}\right)}{t}\right]$$

$T0 = 1.019\times 10^{10}$ $\quad \tau a := \left[\left(\frac{1}{\tau}\right)+(T0)\right]^{-1}$ $\quad \tau a = 9.891\times 10^{-12}$

$$T2 := \left(\frac{1}{t\cdot w}\right)\cdot\left[\frac{(1-R2)\cdot\cos(\theta2)^2\cdot\left[\frac{\cos\left(\theta2^2\right)\cdot\left(-2\cdot E\left(5,\alpha\cdot\frac{w}{\cos(\theta2)}\right)+E\left(5,2\alpha\cdot\frac{w}{\cos(\theta2)}\right)+\frac{1}{4}\right)}{\alpha^3}+-E\left(3,\alpha\cdot\frac{w}{\cos(\theta2)}\right)\cdot\frac{w^2}{\alpha}\right]}{2\alpha}+\frac{(1-R1)\cdot\cos(\theta1)^2\cdot\left[\frac{\cos\left(\theta1^2\right)\cdot\left(-2\cdot E\left(5,\alpha\cdot\frac{w}{\cos(\theta1)}\right)+E\left(5,2\alpha\cdot\frac{w}{\cos(\theta1)}\right)+\frac{1}{4}\right)}{\alpha^3}+-E\left(3,\alpha\cdot\frac{w}{\cos(\theta1)}\right)\cdot\frac{w^2}{\alpha}\right]}{2\alpha}+\frac{(R2+R1)\cdot\left[-E(3,w\alpha)\cdot\left(\frac{w^2}{\alpha}\right)+\frac{1\cdot\left(-2E(5,\alpha\cdot w)+E(5,2\alpha\cdot w)+\frac{1}{4}\right)}{\alpha^3}\right]}{2}+\frac{3\cdot\left(E(5,w\alpha)-\frac{1}{4}\right)}{\alpha^3}+\left(\frac{E(3,\alpha\cdot w)\cdot w^2}{2\alpha}\right)+\frac{w\cdot\left(2E(4,\alpha\cdot w)+\cdots\right)}{\alpha^2}\right.$$

$T2 = 3.087$ $\quad Da := Dm - T2$ $\quad La := \sqrt{Da\cdot\tau a}$ $\quad La = 9.466\times 10^{-5}$

$Da = 906.004$ $\quad \mu := \frac{Da}{.025}$ $\quad \mu = 3.624\times 10^{4}$

LIST OF REFERENCES

1. Sze, SM. *Semiconductor Devices*. Wiley&Sons, 2002.
2. Bolognesi, C.R. et al. *Appl. Phys. Lett.* **86**, 253506-1-3, (2005).
3. Crowe, T.W., et al., "GaAs Schottky diodes for THz mixing applications," *Proc. IEEE.* **80**, 1827, (Nov 1992).
4. Jae-Sung Rieh, et al. *IEEE Transactions on Microwave Theory and Techniques.* **52**, no. 10, (Oct 2004).
5. Woodall, J. et al. "An InAs Based Transistor Approach to Terahertz Electronics including Improved GaAlAs/GaAs HBTs."[electronic bulletin board for research laboratory] (cited 6 Dec,2005);available at http://www.eng.yale.edu/faculty/vita/Woodall_lab.htm
6. Haegel, N.M., Fabbi, J.D. and Coleman, M.P., Appl. *Phys. Lett.* **84,** 1329 (2004).
7. Haegel, N.M., D.R. Luber, F.M. Bradley, M. Talmadge and M.P. Coleman. "Imaging Transport for the Determination of Minority Carrier Diffusion Length." submitted to Review of Scientific Instruments, September 2005.
8. Luber, D.R., Bradley, F.M. and Haegel, N.M.,"Imaging Transport for the Determination of Minority Carrier Diffusion Length." submitted to *Appl. Phys. Lett.,* August 2005
9. Lowney, J.R., Bennett, H.S., *J. Appl. Phys.* **69,** (10), 7102, (1991).

10. DARPA, Broad Agency Announcement 99-15 "Terahertz Technology for Sensing and Satellite Communications" from the *Commerce Business Daily*, Issue No. 2243, 1998.

11. Brisar, John, “Light Emitting Polymers on Flexible Substrates for Naval Firefighting Applications”. Master’s Thesis, Naval Postgraduate School, 2005.

12. Yacobi, B. G. and D. B. Holt, *Cathodoluminescence Microscopy of Inorganic Solids*, (Plenum, New York, 1990), p. 59 and references therein.

13. Kayana, K. and Okayama, S., *J. Appl. Phys.* **5**, 43 (1972).

14. Talmadge, M., Internal Haegel laboratory Report. July, 2005.

15. Donolato & Venturi, “Influence of Generation Distrbution on the Calculated EBIC Contrast of Line Defects”, *Phy. Stat. Sol.(a)*, **78**, 377 (1982).

16. Arfken, G.B, Weber, H.J., *Mathmatical Methods for Physicists.* (Academic Press, San Diego, CA, 2001), pg. 554.

17. Freeman, Will. “Imaging Transport: Optical Measurements of Diffusion and Drift in Semiconductor Materials and Devices.” Master’s Thesis, Naval Postgraduate School, September, 2004.

18. Possin, G.E. & Norton, J.F., *Scanning Electron Microscopy 1975*, (IIT Res. Inst. Chicago, 1975), pg. 475.

19. Luber, DR & Haegel, NM. “Direct Imaging of Electron Beam Interaction Region,” submitted for review Appl. Phys. Lett., 2005.

20. Goldstein, Joseph, et al. *Scanning Electron Microscopy and X-Ray Microanalysis, Third Edition* (Plenum, New York, 2002).

21. Everhart, E., Herzog, R.F., Chang,M.S. and DeVore, W.J. In *Proceedings of the 6th International Conference on X-Ray Optics and Microanalysis* (G. Shinoda, K. Kohra and T. Ichinokawa, eds.), (University of Tokyo Press, Tokyo, 1972). p. 81.

22. Boone, Tom. “High-Speed Optical Modulation Techniques incorporating heavy p-type doping and lateral drift developed in Gallium Arsenide.” PHD Dissertation, Yale University. May, 2004.

23. Bennett, H. S., *J. Appl. Phys*. **92**, 8 (2002).

24. Harmon, E.S., Lovejoy, M.L., Melloch, M.R. and Lundsfrom, M.S., “Experimental observations of a minority electron mobility enhancement in degenerately doped p-type GaAs,” *Appl.Phys.Lett*. **63**, (4), (1993).

25. Kim, D.M., et al., *J. Appl. Phys*. **69**, 7102 (1991).

26. Lovejoy, M.L., et al., Appl. Phys. Lett. **61**, 822 (1992).

27. Furuta, T. and Yoshii, A., *Appl. Phys. Lett*. **59**, 3607 (1991).

28. Harmon, E.S., Melloch, M.R., Lundstrom, M.S., and Lovejoy, M.L., *Appl. Phys. Lett.* **83**, 537 (1993).

29. Casey, H.C., SpringThorpe, A.J., “Nonconventional electron diffusion current in GaAs/AlGaAs N-p-n

heterojunction bipolar transistors with heavily doped base layers”, *J. Appl. Phys.* **85,** 6 (1989).

30. Renaud, Ph., Raymond, F., Bensaid, B., and Verie, C., *J. Appl. Phys.* **71** (4),(1992).

31. Badescu, V. and Landsberg, P.T., *Semicond. Sci. Technol.* **8,** 1267, (1993).

32. Patkar, Lundstrom, and Melloch, *J. Appl. Phys.*, **78**, (4), (1995).

33. Casey, Jr., Sell, Wecht, *J. Appl. Phys.,* **46**, (1) (1975).

34. Asbeck, P., *J. Appl. Phys.*, **48**, (2), (1977).

35. Pedrotti, Leno, Pedrotti, Introduction To Optics,(New Jersey, Prentice Hall, 1993), pg.514.

INITIAL DISTRIBUTION LIST

1. Defense Technical Information Center
   Ft. Belvoir, Virginia

2. Dudley Knox Library
   Naval Postgraduate School
   Monterey, California

3. Professor Nancy M. Haegel
   Naval Postgraduate School
   Monterey, CA

4. Professor James Luscombe
   Naval Postgraduate School
   Monterey, CA

5. Thomas Boone
   Hitachi Global Storage
   San Jose, CA

6. Dave Luber
   Headquarters United States Marine Corps
   Washington, DC

7. Rear Admiral Joe Kernan
   United States Special Operations Command
   Tampa, FL